Controlling Triplet-Pair Formation in Acene-Bridged Trimers through Locally Excited–Charge-Transfer State Mixing

*Ebin Sebastian[a], Daniel G.Congrave[b,c†], Jeroen Royakkers[b†], Stephanie Montanaro[b], Huaxi Huang[d], Ashish Sharma[a], Julia Osmólska[a], He Zhu[b], Chanakarn Phansa[a], Jurjen Winkel[a], Oliver Millington[b], Murad J. Y. Tayebjee[e], Luis M. Campos[d], Hugo Bronstein[*a,b], Akshay Rao[*a]*

[a]*Cavendish Laboratory, University of Cambridge, Cambridge, CB3 0HE, United Kingdom*
[b]*YusufHamied Department of Chemistry, University of Cambridge, Cambridge, CB2 1EW, United Kingdom*
[c]*Chemistry Research Labloratory, University of Oxford, Oxford, OX1 3TA, United Kingdom*
[d]*Department of Chemistry, Columbia University, New York, New York 10027, United States*
[e]*School of Photovoltaic and Renewable Energy Engineering UNSW Sydney, Sydney, 2052, NSW, Australia*
† These authors contributed equally

*E-mail: ar525@cam.ac.uk, Email: hab60@cam.ac.uk

Electronic Supplementary Information (ESI)

Table of Contents

Section 1: Materials and Methods

All chemicals were obtained from commercial suppliers and used as received without further purification. All reactions were carried out in oven-dried glassware prior to use. 1H NMR spectra were recorded on a 400 MHz Avance III HD Spectrometer, 400 MHz Smart Probe Spectrometer or a 500 MHz DCH Cryoprobe Spectrometer in the stated solvent using residual protic solvent as the internal standard. 1H NMR chemical shifts are reported to the nearest 0.01 ppm. The coupling constants (J) are measured in Hertz. Mass spectra were obtained using a Waters LCT, Finnigan MAT 900XP or Waters MALDI micro-MX spectrometer at the Department of Chemistry, University of Cambridge. Reactions requiring an inert atmosphere were carried out under argon. Thin layer chromatography (TLC) was carried out on silica gel and visualized using UV light (254, 365 nm). Flash chromatography was carried out on a Biotage® Isolera automated flash chromatography machine on 60-micron silica gel cartridges purchased from Biotage®. Preparative HPLC was carried out on a Phenomenex® lux ic-5 column on an Agilent® 1260 Infinity II.

All commercial chemicals were of ≥95% purity and were used as received without further purification. Anhydrous solvents were purchased from Sigma Aldrich or Acros Organics and used as received. All optical measurements were carried out in 1 mm pathlength quartz cuvettes. Samples were prepared in a nitrogen-atmosphere glovebox using degassed, anhydrous solvents. Cuvettes were sealed prior to measurements with a PTFE cap, PTFE tape, and parafilm, to ensure the absence of oxygen inside the samples.

1.1 Computational Analysis

Geometry optimizations of all molecular system under the study were carried out using density functional theory (DFT) as implemented in the Gaussian 16 program package[1]. The B3LYP functional combined with the 6-31G(d,p) basis set was employed for all optimizations. Vertical excitation energies and oscillator strengths were calculated employing time-dependent DFT (TD-DFT) at the ωB97XD functional and def2svp level of theory. The frontier molecular orbitals (FMO) were obtained from the generated cube files of energy calculations. To reduce computational cost, all isopropyl alkyl chains in the studied molecules were replaced by methyl groups during the calculations.

1.2 Steady-state absorption and photoluminescence

Steady-state absorption across the UV/Vis/NIR spectral regions were carried out using a Shimadzu UV3600Plus spectrometer. Steady-state photoluminescence spectra were measured using an Edinburgh Instruments FLS1000-DD-stm spectrometer, comprised of a 450-xenon lamp for excitation and a FLS1000 double excitation and double emission monochromator. The emissions were detected using a PMT-980 detector.

1.3 Time-resolved photoluminescence

Time-resolved photoluminescence was carried out on an Edinburgh Instruments FLS1000-DD-stm spectrometer. The time-resolved photoluminescence of the TIPS-BT0, TIPS-TAT, Encap-TA and Encap-TA molecules (ns timescale) was measured using time correlated single photon counting (TCSPC). Samples were excited with a pulsed 505 nm EPL-505, diode laser at a 2 MHz repetition rate (~60 ps pulsewidth). Pump scatter from the laser excitation was filtered out using an appropriate Thorlabs long-pass filter in the emission path. The photoluminescence was directed through an FLS1000 double emission monochromator and detected by a PMT-980 detector in TCSPC mode. The instrument response was determined using light scattered off a piece of scratched glass at the excitation wavelength, giving a value of 137 ps.

1.4 Photoluminescence quantum efficiency (PLQE)

PLQE measurements were carried out inside a Spectralon coated integrating sphere following the procedure of de Mello et al.[2] Measurements were taken at room temperature using a temperature and current controlled 405 nm Thorlabs continious wave laser diode as the excitation source. Light from the experiment was collected using an optical fiber connected to an Andor Kymera 328i Spectrometer housing a DU420A Silicon CCD detector. Setup calibration was performed using a Bentham 610 QTH calibration source. PLQE calculations were performed as described by de Mello et al.[2]

1.5 Femtosecond transient absorption (fsTA)

Femtosecond transient absorption (TA) measurements were performed on a HARPIA system (Light Conversion). The fundamental output of a PHAROS femtosecond laser (1030 nm, 10 kHz; Light Conversion) was split to provide pump and probe paths. Tunable pump pulses were generated using an ORPHEUS optical parametric amplifier (Light Conversion) operated in a collinear geometry. For the probe, UV–blue, white-light continuum (≤ ~520 nm) was produced by first frequency-doubling the 1030 nm beam to 515 nm in a β-BaB_2O_4 (BBO) crystal and then focusing the 515 nm pulses into a sapphire plate. For longer-wavelength coverage (> ~520 nm; visible–NIR), the 1030 nm fundamental was focused directly into sapphire to generate the supercontinuum. Pump and probe were spatially and temporally overlapped at the sample, with the delay controlled by the HARPIA delay line. To suppress rotational-diffusion artifacts, the pump polarization was set to the magic angle (54.7°) relative to the probe. Transient signals were recorded as ΔA (λ, t).

1.6 Nanosecond transient absorption (nsTA)

A 532 nm pump beam was generated by the second harmonic, respectively, of a Q-switched Nd:YVO4 (1 ns pump length, Advanced Optical Technologies Ltd AOT-YVO-25QSPX) laser. A LEUKOS Disco 1 UV low timing jitter supercontinuum laser (STM-1-UV) was used to generate the probe beam. The probe beam was split by a 50% beam splitter into a reference and probe, and both were focused and directed through the sample – only the probe beam interacted, i.e. was overlapped, with the pump beam. This allows for correction of any shot-to-shot fluctuations. A pair of line image sensors (Hamamatsu, G11608) mounted on a spectrograph (Andor Solis, Shamrock SR-303i) were used to detect the signal, using a custom-built board from Entwickslungsbüro Stresing to read out the signal. The delay was controlled electronically for all nanosecond transient absorption measurements, and every second pump pulse is omitted. The average fractional differential transmission (ΔT/T) of the probe is calculated after each time delay following the collection of 1000 shots.

1.7 Global Analysis

Global analyses of the fsTA and nsTA spectra were performed using the Glotaran software.[3,4] The workflow explicitly accounts for the instrument response function (IRF) and the group-velocity dispersion (chirp) of the white-light continuum, enabling extraction of dispersion-corrected spectra and kinetic parameters from a simultaneous fit of all wavelengths.

First, the spectra were analysed using a sequential (global) model to obtain evolution-associated difference spectra (EADS/EAS). In this approach, all wavelengths are fitted concurrently with a chain of exponentially decaying components, yielding time constants and the corresponding EADS that describe how the spectrum evolves. Importantly, EADS/EAS are model-dependent spectral components and the associated time constants do not necessarily correspond to distinct physical/chemical species; rather, they provide a compact description of spectral evolution on different timescales.

To connect the observed singlet fission kinetics to a physically motivated mechanism, the fsTA data of **TIPS-TAT** and **TIPS-BT0** were additionally analysed using a target model (Figure S1a), in which the population dynamics are constrained by an explicit kinetic network (e.g., $S_1 \rightleftarrows TT \rightarrow G$). This analysis returns species-associated spectra (SAS) for the compartments in the kinetic scheme together with microscopic rate constants, enabling assignment of the fsTA features to specific intermediates within the assumptions of the model. The fsTA and nsTA datasets were used to guide and validate the kinetic interpretation through the sequential EADS/EAS analysis, while the target-model fitting was restricted to the psTA time window where the relevant interconversion dynamics are most directly resolved.

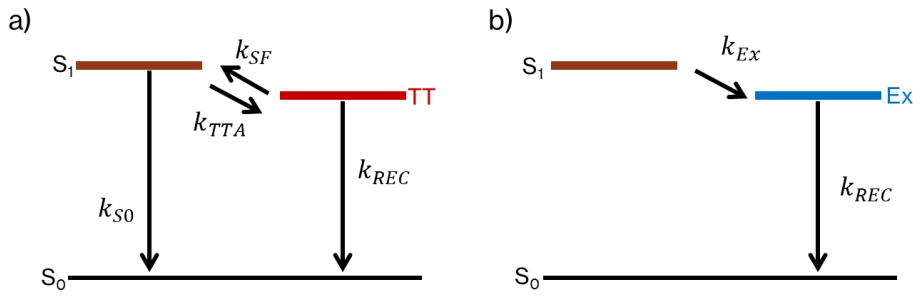

Figure SI1: Kinetic schemes used for analysis of the fsTA data in toluene (TOL). **(a)** Target-analysis model applied to **TIPS-BT0** and **TIPS-TAT**. **(b)** Sequential global-analysis model applied to Encap-TAT, yielding evolution-associated difference spectra (EADS).

In Fig. SI1a, the population of S_1 and TT can be described using the following kinetic equations,

$$\frac{d[S_1]}{dt} = -k_{SF}[S_1] - k_{SF}[S_1] + K_{TTA}[TT] \quad \text{(S1)}$$

$$\frac{d[TT]}{dt} = k_{SF}[S_1] - k_{TTA}[TT] - k_{REC}[TT] \quad \text{(S2)}$$

Here, k_{SF} is the singlet fission rate and k_{TTA} is the back reaction, k_{S0} is the singlet depopulation to ground state and k_{REC} is the loss of TT state.

In Figure SI1b, the population of S_1 and Ex can be described using the following kinetic equations,

$$\frac{d[S_1]}{dt} = -k_{Ex}[S_1] \quad \text{(S3)}$$

$$\frac{d[Ex]}{dt} = -k_{REC}[Ex] \quad \text{(S4)}$$

Here, k_{Ex} is the Excimer formation rate and k_{REC} is depopulation rate of Excimer state to ground state.

1.8 Determination of State Energies and Charge-Transfer (CT) State Estimation

The vertical ionization potential (IP) and electron affinity (EA) of each molecular fragment, **Encap-T**, **TIPS-T** and **TIPS-A**, were obtained from single-point DFT calculations on the optimized neutral geometries (B3LYP/6-31G(d,p)) . Three total energies were computed for each molecule: the neutral ground state (E_{GS}), the cation (E_{Cation}), and the anion (E_{anion}). All energies were reported in Hartree and subsequently converted to electronvolts using the relation 1 Hartree=27.2114 eV.

The IP and EA were extracted as:

$$IP = E_{Cation} - E_{GS} \quad \text{(S5)}$$

$$EA = E_{GS} - E_{Anion} \quad \text{(S6)}$$

The vertical gas-phase CT excitation energy for a donor–acceptor pair was then estimated using:

$$E_{CT}^{(gas)} = IP_{donor} - EA_{acceptor} \quad \text{(S7)}$$

To account for Coulomb stabilization of the electron–hole pair in the solvent environment, a simple point-charge model was employed:

$$C = \frac{-e^2}{4\pi\varepsilon_0}\left(\frac{1}{\varepsilon_S r_{AD}}\right) \quad \text{(S8)}$$

here ε_S is the static dielectric constant of the solvent (2.38 for toluene), r_{AD} is the centre-to-centre separation between the donor and acceptor (12.47 A˚for **Encap-TA** and **TIPS-TA** and 13.69A˚for **TIPS-BT0**), and $\frac{-e^2}{4\pi\varepsilon_0}$ =14.3996 eV\A˚

The optical CT energy was then estimated as:

$$E_{CT}^{(opt)} = E_{CT}^{(gas)} + C \qquad \text{(S9)}$$

This approach neglects geometry relaxation in the charged states and higher-order polarisation effects but provides a reasonable first order estimate of the CT excitation energy suitable for comparison with experimental absorption onsets.

1.9 Columbic coupling

To determine the Coulombic excitonic coupling between the two chromophores in our dimers, we performed TDDFT calculations on each monomer unit at the ground-state geometry (extracted from the dimer) obtained from DFT optimizations. Vertical excitations were computed at the ωB97X-D/def2-SVP level of theory.[5–8] The resulting transition densities were mapped to atomic transition charges using the Transition Charges from Electrostatic Potential (TrEsp) scheme as implemented in Multiwfn v3.7.83 (ESP-fit of the transition density rather than Mulliken populations).[9,10]

The Coulombic exciton coupling J_{coul} between chromophore a and b was then evaluated as

$$J_{coul} = \frac{1}{4\pi\varepsilon_0}\sum_i\sum_j \frac{q_i^{(a)} q_j^{(b)}}{\left|r_i^{(a)} - r_j^{(b)}\right|} \qquad \text{(S10)}$$

where $q_i^{(a)}$are the (scaled) **transition charges** on the atom i of chromophore a, $r_i^{(a)}$ are their position vectors, and ε_0 is the vacuum permittivity.

Notes. (i) The TrEsp J_{coul} captures the long-range Coulomb component of the excitonic coupling; short-range exchange/overlap and CT-mediated contributions are not included and are treated separately (see section, 1.10). (ii) Geometry-optimised dimer structures used for Eq. (S10) were obtained from our DFT calculations; monomer transition densities were computed at the dimer-embedded (frozen) monomer geometries to preserve the correct intermolecular geometry

1.10 Charge-transfer coupling calculations

The electron (e) and hole (h) transfer integrals were computed using a fragment orbital projection scheme implemented in PySCF (v2.7.0)[11]. For each monomer, single-point DFT calculations were performed at the PBE0/def2-SVP level to obtain the frontier orbitals (HOMO and LUMO). These orbitals were then projected into the atomic orbital (AO) basis of the full dimer, and the dimer was computed at the same level of theory.

The Kohn–Sham Fock matrix F and AO overlap matrix S_{AO} of the dimer were used to construct the effective Hamiltonian in the non-orthogonal fragment orbital basis[12]:

$$H = \Phi^{\dagger} F \Phi, \qquad S = \Phi^{\dagger} S_{AO} \Phi \qquad \text{(S11)}$$

where Φ denotes the matrix of selected fragment orbitals. To remove non-orthogonality between monomer orbitals, Löwdin orthogonalization[13] was applied:

$$H_{eff} = S^{-1/2} H S^{-1/2} \qquad \text{(S12)}$$

The off-diagonal block elements of H_{eff} gives the transfer integrals:

$$t_e = H_{eff}^{AB}(LUMO, LUMO) \qquad \text{(S13)}$$

$$t_h = H_{eff}^{AB}(HOMO, HOMO) \qquad \text{(S14)}$$

$t_e$is electron transfer integrals (LUMO–LUMO) and t_h is the hole (HOMO–HOMO) transfer integrals, respectively. All energies were obtained in Hartree and converted to spectroscopic units using 1 Ha = 27.2114 eV = 27211.4 meV = 219474.6 cm^{-1}

1.11. Local-excitation (LE)–Charge-Transfer (CT) Mixing Analysis

The local-exciton (LE)-charge-transfer (CT) mixing analysis is a computational method used to determine the composition of excited electronic states in molecular systems, particularly heterodimers. It employs a four-state diabatic Hamiltonian approach to quantify the contribution of localized LE states and delocalized charge-transfer (CT) states to the overall character of the adiabatic excited states.

The analysis is based on a diabatic basis set composed of four key states:

$|S_1S_0\rangle$: Represents a **local excitation (LE)** on chromophore A, with chromophore B remaining in its ground state (S0).

$|S_0S_1\rangle$: Represents an **LE** on chromophore B, with chromophore A in its ground state.

$|CA\rangle$: Represents a **charge-transfer (CT)** state where chromophore A is a cation (A^+) and chromophore B is an anion (B–).

$|AC\rangle$: Represents a **CT** state where chromophore A is an anion (A–) and chromophore B is a cation (B+).

The diabatic Hamiltonian (H) is a 4×4 matrix that describes the interactions and energies of these four states. It's built using a set of specific parameters, LE energies (E_A,E_B): The diagonal elements corresponding to the LE states, TDDFT 0-0 transition energies. CT state energies ($E_{CT(CA)}$, $E_{CT(AC)}$): The diagonal elements for the CT states, determined via DFT calculations (see section 1.8, SI). LE-LE Coulombic coupling (J_{Coul}): Represents the electrostatic interaction between the two LE states. It is a measure of how the excitation on one chromophore influences the excitation on the other. See section 1.9, SI. Hole transfer integrals (t_h): Describe the transfer of a positive "hole" between the chromophores. Electron transfer integrals (t_e): Describe the transfer of an electron between the chromophores.

The diabatic Hamiltonian was defined as:

$$H = \begin{pmatrix} E_A & J_{Coul} & t_e & t_h \\ J_{Coul} & E_B & t_h & t_e \\ t_e & t_h & E_{CT(CA)} & 0 \\ t_h & t_e & 0 & E_{CT(AC)} \end{pmatrix} \quad \text{(S15)}$$

To find the adiabatic excited states, the diabatic Hamiltonian is diagonalised. This process yields the **eigenvalues**, which correspond to the energies of the adiabatic states, and the **eigenvectors**, which describe the composition of each adiabatic state as a linear combination of the diabatic states.

Diagonalization of H yields the adiabatic excited states $|\psi_i\rangle$ and their energies E_i. Each adiabatic state is expressed as:

$$|\psi_i\rangle = a^{(i)}_{S_1S_0}\,|S_1S_0\rangle + a^{(i)}_{S_0S_1}\,|S_0S_1\rangle + b^{(i)}_{CA}\,|CA\rangle + b^{(i)}_{AC}\,|AC\rangle \quad \text{(S16)}$$

Where, $a^{(i)}$ terms are amplitudes for the LE basis states, and $b^{(i)}$terms are amplitudes for the charge-transfer basis states.

The LE fraction for a given adiabatic state $|\psi_i\rangle$ is calculated by summing the squared coefficients of the LE states in its eigenvector:

$$\text{LE fraction} = |a^{(i)}_{S_1S_0}|^2 + |a^{(i)}_{S_0S_1}|^2 \quad \text{(S17)}$$

Similarly, the CT fraction is the sum of the squared coefficients of the CT states:

$$\text{CT fraction} = |b_{CA}^{(i)}|^2 + |b_{AC}^{(i)}|^2 \quad \text{(S18)}$$

These fractions, ranging from 0 to 1, quantify the character of each adiabatic state, indicating whether it is primarily localized (LE) or delocalized (CT).

1.12. Computational Details for Excitonic-Coupling Simulations

To model the absorption features of **Encap-TA**, we employed a full vibronic Frenkel–exciton Hamiltonian with the following key steps,

Vibronic Hamiltonian Construction

For each vibrational quantum number v (up to v_{max}=10v), we built the 2×2 block

$$H_v = \begin{pmatrix} E_A + v\omega & J \\ J & E_B + v\omega \end{pmatrix} \quad \text{(S19)}$$

where E_A and E_B are the 0–0 transition energies of chromophore and bridge (in eV), ω is the common vibrational quantum spacing, and J is the electronic coupling. Diagonalization yields the vibronic eigenenergies,

$$E_{\pm}(v) = \frac{E_A+E_B}{2} + v\omega \pm \sqrt{(\frac{E_A-E_B}{2})^2 + J^2} \quad \text{(S20)}$$

Franck–Condon Weighting

Each vibronic transition is weighted by the Huang–Rhys–derived Franck–Condon factor

$$FC(v) = e^{-s}\frac{S^v}{v!} \quad \text{(S21)}$$

where S is the Huang–Rhys parameter.

Oscillator Strength and Lineshape

The transition dipole for each eigenstate is computed as the coherent sum of,

$$\mu_{eff} = C_1\mu_A + C_2\mu_B \quad \text{(S22)}$$

Where, μ_1 and μ_2 the monomer dipoles and (C_1, C_2) the components of the eigenvector. The resulting oscillator strength is

$$I_{\pm}(v) \propto FC(v)|\mu_{eff}|^2 \quad \text{(S23)}$$

Each line is broadened by convolution with a normalized Lorentzian $\frac{1}{\pi}\frac{\gamma}{(\Delta E)^2+\gamma^2}$, using γ ≃ 0.08 eV

A weak CT band was modelled as a single Lorentzian centred at E_{CT} with width γ_{CT} and small amplitude to account for the experimentally observed shoulder. All spectra were computed on a uniform energy grid (2.0–3.5 eV) and converted to wavenumbers (cm^{-1}) for plotting alongside experimental data. A twin top axis displays the corresponding wavelengths (nm).

By adjusting E_A, E_B, ω, S, J, μ_A, μ_B, and γ, we achieved excellent agreement between the simulated total (upper + lower branch + CT) spectrum and the measured **Encap-TA** absorption. The best-fit electronic coupling J ≈ 0.040 eV (≈ 332 cm^{-1}) quantitatively confirms intermediate H-type excitonic mixing in the single-arm dimer.

1.13. Estimation of Yields of Triplet-Pair States and Isolated Triplets.

To quantify the degree of triplet-pair formation within the reversible singlet fission (SF) manifold, the early-time dynamics are treated as a two-state interconversion between the initially prepared singlet excited state (S_1) and the correlated triplet-pair state (^{1}TT):

$$S_1 \underset{k_{-SF}}{\overset{k_{SF}}{\leftrightarrows}} {}^1(\mathrm{TT}) \qquad \text{(S24)}$$

Here, k_{SF} is the forward rate constant for $S_1 \rightarrow {}^1(TT)$, and k_{-SF} is the back reaction rate constant for ${}^1(TT) \rightarrow S_1$. Under the simplifying approximation fthat decay of S_1 to the ground state is slow compared with the reversible $S_1 \rightleftharpoons {}^1(TT)$ equilibration, the equilibrium constant for the SF interconversion is given by:

$$K_{SF} = \frac{[TT]_{eq}}{[S_1]_{eq}} = \frac{k_{SF}}{k_{-SF}} \qquad \text{(S25)}$$

Therefore, the singlet fission yield given by,

$$\phi_{TT} = \frac{[TT]_{eq}}{[TT]_{eq}+[S_1]_{eq}} = \frac{K_{SF}}{K_{SF}+1} \qquad \text{(S26)}$$

For TIPS-BT0, k_{SF} = 0.7194 ps^{-1} and k_{-SF} = 0.0225 ps^{-1} and for TIPS-TAT, k_{SF} = 0.0892 ps^{-1} and k_{-SF} = 0.0018 ps^{-1}. Hence singlet fission is ϕ_{TT} = 96.97 % (TIPS-BT0) and ϕ_{TT} = 98.02 % (TIPS-TAT).

Isolated triplet quantum yield was calculated by assuming that absorption cross section of a triplet-pair state is equal to the absorption cross section of two triplets. This is equivalent to treating the singlet fission yields 96.97 % (TIPS-BT0) and 98.02 % (TIPS-TAT) as equivalent to a peak triplet yield of 193.94 % (TIPS-BT0) and 196.04 % (TIPS-TAT). The yield of isolated triplets may then be determined by comparing the height of the 'triplet plateau' that is associated with those states to the height of the peak of the triplet/triplet-pair PIA signal. The plateau intensities are ~8% for TIPS-BT0 and ~30% for TIPS-TAT. This would indicate isolated triplet yields of ~15.51%, and ~58.77% respectively.

1.14. Electrochemistry (Cyclic Voltammetry)

Cyclic voltammetry (CV) measurements were carried out using a conventional three-electrode configuration consisting of a glassy carbon working electrode (polished prior to use), a platinum wire counter electrode, and a non-aqueous Ag/Ag^+ reference electrode. The supporting electrolyte was 0.1 M tetrabutylammonium hexafluorophosphate (Bu_4NPF_6) in anhydrous dichloromethane (CH_2Cl_2). Sample solutions were prepared under an inert atmosphere, purged with argon for 30 min prior to measurement, and maintained under argon during data acquisition. Cyclic voltammograms were recorded for at least five consecutive cycles at a scan rate of 0.10 V s^{-1}. Potentials are reported versus Ag/Ag^+; where indicated, ferrocene was added as an internal standard, and potentials were referenced to the Fc/Fc^+ couple (Figure S30).

Section 2: Tables

Table S1: UV-vis and Fluorescence Spectroscopic Data of **TIPS-BT0**, **TIPS-TAT** and **Encap-TAT** Measured in Toluene at Room Temperature.

	TIPS-BT0	**TIPS-TAT**	**Encap-TAT**	**Encap-TA**
$\lambda_{abs}(FE1)$, nm/cm^{-1}	~550 /18,182	~547/ 18,282	~514/ 19,445	~512/ 19,531
$\lambda_{abs}(FE2)$, nm/cm^{-1}	-	~471/ 21,230	~469/ 21,320	~453/ 22,076
$\lambda_{abs}(CT)$, nm/cm^{-1}	~429 /23,310	~408/ 24,510	~398/ 25,126	~385/ 25,974
λ_{PL}, nm/cm^{-1}	~556 /17,986	~556/17,986	~571/ 17,513	~555/ 18,018
$\Delta\tilde{\nu}_{Stokes}$, nm/cm^{-1}	~6 /196	~9/ 296	~57/ 1,932	~43/1,513
ϕ_{PL}, %	~0.3	~38.5	~80.5	~59.7
τ_{PL}, ns	8.50 (99.73 %) 31.99 (0.27 %)	11.13 (91.50 %) 96.08 (8.50 %)	10.63 (91.77 %) 89.98 (8.23 %)	7.84 (96.80 %) 25.01 (3.20 %)

Table S2: Oscillator strength for different transitions of **TIPS-T**, **Encap-T** and **TIPS-A** calculated at TD-wB97XD/def2svp level of theory. Transition dipole moment (μ) of **TIPS-T** is 1.750 a.u., **Encap-T** is 1.1940 a.u. and **TIPS-A** is 1.9828 a.u.

Molecule	Excitation		Energy (eV)	Wavelength (nm)
	State	Oscillatory Strength		
TIPS-T	S_1	0.3306	2.4574	504.54
	S_2	0.0230	3.5837	345.97
	S_3	0.0957	3.8176	324.77
	S_4	0.0127	4.2468	291.95
Encap-T	S_1	0.1465	2.746	451.52
	S_2	0.0031	3.6679	338.03
	S_3	0.0087	4.1668	297.55
	S_4	0.0010	4.4428	279.07
TIPS-A	S_1	0.4869	2.9833	415.59
	S_2	0.0135	3.8653	320.76
	S_3	0.0004	4.6581	266.17
	S_4	0.0000	4.7014	263.72

Table S3: Oscillator strength for different transitions of **TIPS-BT0**, **TIPS-TAT** and **Encap-TAT** calculated at TD-wB97XD/def2svp level of theory.

Molecule	Excitation		Energy (eV)	Wavelength (nm)
	State	Oscillatory Strength		
TIPS-BT0	S_1	0.5326	2.4265	510.95
	S_2	0.0419	2.4435	507.41
	S_3	0.000	3.4119	363.38
	S_4	0.5085	3.4852	355.74
TIPS-TAT	S_1	0.4429	2.4342	509.34
	S_2	0.1488	2.4355	509.07
	S_3	0.3611	2.8597	433.55
	S_4	0.430	3.4375	360.69
Encap-TAT	S_1	0.2212	2.6761	463.31
	S_2	0.1285	2.7003	459.15
	S_3	0.2842	2.8606	433.42
	S_4	0.3553	3.4564	358.71

Table S4: Oscillator strength for different transitions of **TIPS-TA** and **Encap-TA** calculated at TD-wB97XD/def2svp level of theory.

Molecule	Excitation		Energy (eV)	Wavelength (nm)
	State	Oscillatory Strength		
TIPS-TA	S_1	0.2985	2.4355	509.08
	S_2	0.3669	2.9244	423.96
	S_3	0.0431	3.4573	358.62
	S_4	0.5600	3.6486	339.81
Encap-TA	S_1	0.1575	2.6794	462.73
	S_2	0.3492	2.9242	423.99
	S_3	0.0621	3.5157	352.66
	S_4	0.2731	3.6624	338.53

Table S5: DFT-calculated total energies (Hartree), ionization potentials (IP), electron affinities (EA), and charge-transfer (CT) energies for the studied donor–acceptor systems. Coulomb term C computed for r_{AD} = 1.2473 nm in toluene (ε_s= 2.38)

Molecule	E_{GS} (Hartree)	E_{cation}(Hartree)	E_{anion}(Hartree)	IP (eV)	EA (eV)
Encap-T	-2003.156914	-2003.965954	-2004.215369	5.196	1.591
TIPS-A	-1509.265152	-1509.054543	-1509.333676	5.731	1.865
TIPS-T	-1662.904915	-1662.706360	-1662.984516	5.403	2.166

Table S6: Estimated CT excitation energies.

Donor	Acceptor	IP_{donor} (eV)	$EA_{acceptor}$(eV)	E_{CT}^{opt}(eV)	$E_{CT}^{opt}(cm^{-1})$
Encap-T	**TIPS-A**	5.1963	1.8646	2.8466	22,959.37
TIPS-A	**Encap-T**	5.731	1.591	3.6549	29,478.74
TIPS-A	**TIPS-T**	5.731	2.1661	3.0798	24,840.25
TIPS-T	**TIPS-A**	5.403	1.8646	3.0533	24,626.51
TIPS-T	**TIPS-T**	5.403	2.1661	2.7950	22,543.18

Table S7; Calculated electronic parameters for the investigated dimers. J_{Coul} denotes the Coulombic excitonic coupling (cm^{-1}), t_e and $t_h$are the electron and hole transfer integrals (cm^{-1}), E_A and E_B are the local excitation energies of monomers A and B (cm^{-1}), and E_{CT}^{CA} and E_{CT}^{AC}epresent the charge-transfer state energies with electron transfer from A→B and B→A, respectively (cm^{-1}).

	TIPS-TA	**Encap-TA**
E_A	18,550.75	20,163.86
E_B	22,409.20	22,409.20
E_{CT}^{CA}	24,626.51	22,959.37
E_{CT}^{AC}	24,840.25	29,478.74
J_{Coul}	-237.5	219.92
t_e	1,369.44	1147.69
t_h	-446.32	-1334.99

Table S8: Key to data table for dimer (homo/hetero) eigenstate calculations.

Sample	S_1S_0	S_0S_1	CA	AC
S_1S_0	E_A	J_{Coul}	t_e	t_h
S_0S_1	J_{Coul}	E_B	t_h	t_e
CA	t_e	t_h	$E_{CT(CA)}$	0
AC	t_h	t_e	0	$E_{CT(AC)}$

Eigensatets

	ψ_1	ψ_2	ψ_3	ψ_4
Sample				
S_1S_0	a(Ex 1)	a(Ex2)	a(Ex3)	a(Ex4)
S_0S_1	a(Ex 1)	a(Ex2)	a(Ex3)	a(Ex4)
CA	b(Ex 1)	b(Ex2)	b(Ex3)	b(Ex4)
AC	b(Ex1)	b(Ex2)	b(Ex3)	b(Ex4)

	ψ_1	ψ_2	ψ_3	ψ_4	
Eigenvalues	**E**(Ex1)	**E**(Ex2)	**E**(Ex2)	**E**(Ex3)	**E**(Ex4)

Table S9: Adiabatic eigenstates of **Encap-TA** expressed in the local diabatic basis (S_1S_0, S_1S_0, CA, AC). Listed are the normalized coefficients, eigenenergies,

	Eigensatets			
	ψ_1	ψ_2	ψ_3	ψ_4
S_1S_0	+0.866783	-0.452504	-0.158300	+0.137364
S_0S_1	-0.284972	-0.780236	+0.534462	-0.156121
CA	-0.382053	-0.430178	-0.816186	+0.053126
AC	+0.146676	+0.037678	-0.152091	-0.976696

	ψ_1	ψ_2	ψ_3	ψ_4
Eigenvalues (cm^{-1})	19359.78	21745.28	24056.15	29849.95

Table S10: Adiabatic eigenstates of **TIPS-TA** expressed in the local diabatic basis (S_1S_0, S_0S_1, CA, AC). Listed are the normalized coefficients and eigenenergy's.

	Eigensatets			
	ψ_1	ψ_2	ψ_3	ψ_4
S_1S_0	+0.976003	-0.039969	+0.162381	+0.139471
S_0S_1	+0.012510	-0.909202	+0.055299	-0.412477
CA	-0.207982	-0.121719	+0.892351	+0.381626
AC	+0.063278	+0.396155	+0.417474	-0.815336

	ψ_1	ψ_2	ψ_3	ψ_4
Eigenvalues (cm^{-1})	18226.95	21742.32	24848.05	25609.39

Table S11: Lifetimes extracted from target/global analysis of fs-TA data using Glotaran.

	TIPS-BT0	TIPS-TAT	Encap-TAT
τ_{SF} or τ_{Ex}	1.39 $\pm$ 0.03 ps	11.2 $\pm$ 0.06 ps	2.95 $\pm$ 0.04 ps
τ_{TTA}	44.37 $\pm$ 0.1 ps	537.6 $\pm$ 0.1 ps	
τ_{TT} or τ_{REC}	8.7$\pm$ 0.4 ns	127.56$\pm$ 1 ns	16.9$\pm$ 0.2 ns

Section 3: Figures

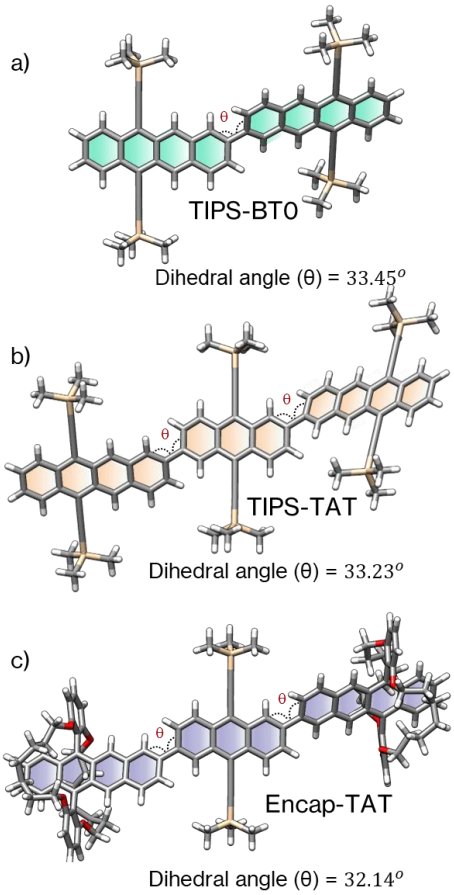

Figure S1. Energy-minimized structures of (a) **TIPS-BT0**, (b) **TIPS-TAT** and (c) **Encap-TAT** calculated at the B3LYP/6-31g(d) level of theory.

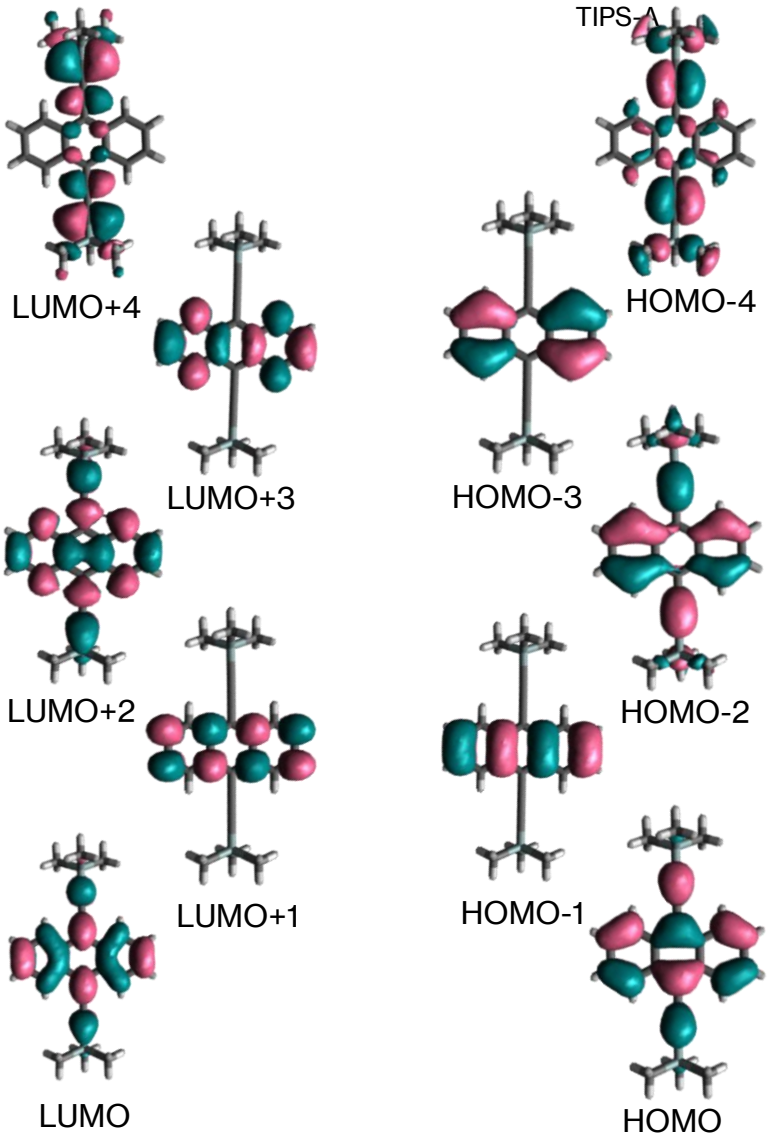

Figure S2. Frontier molecular orbitals of **TIPS-A**.

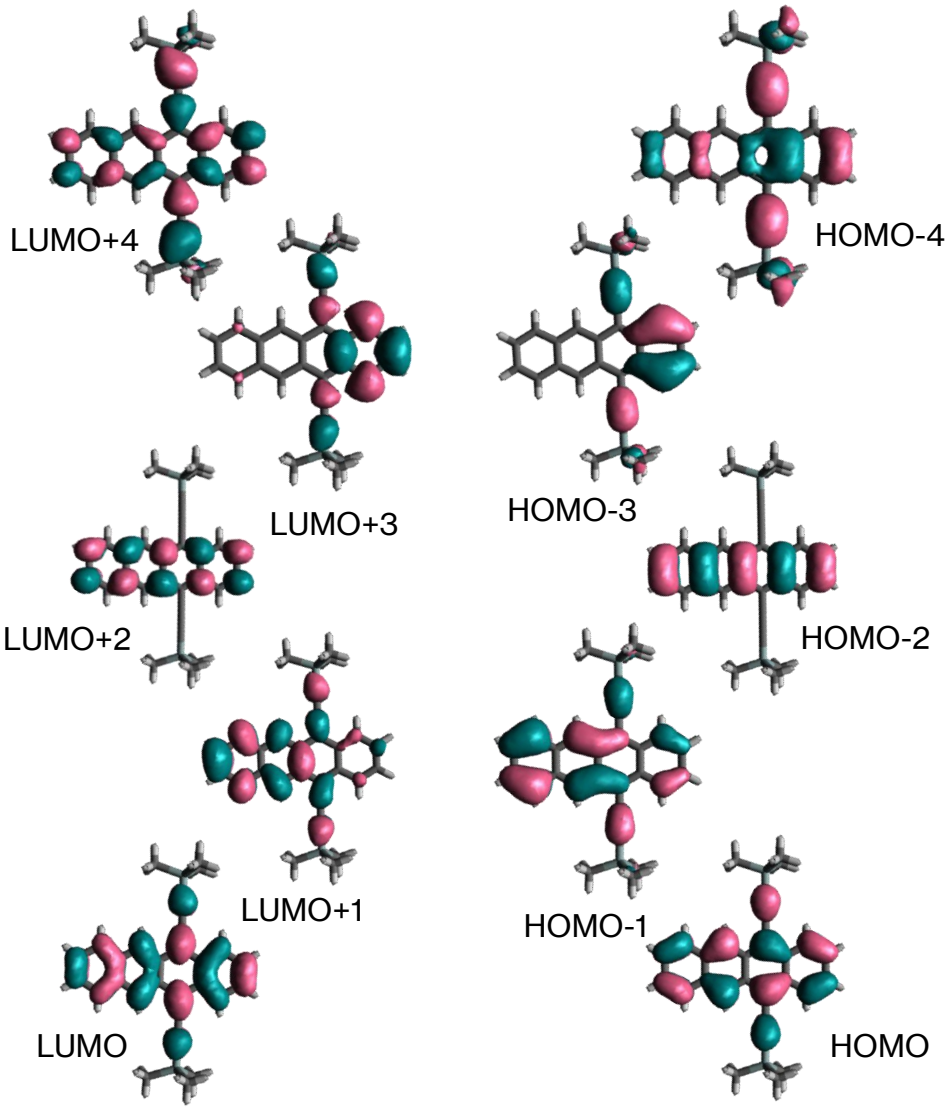

Figure S3. Frontier molecular orbitals of **TIPS-T**.

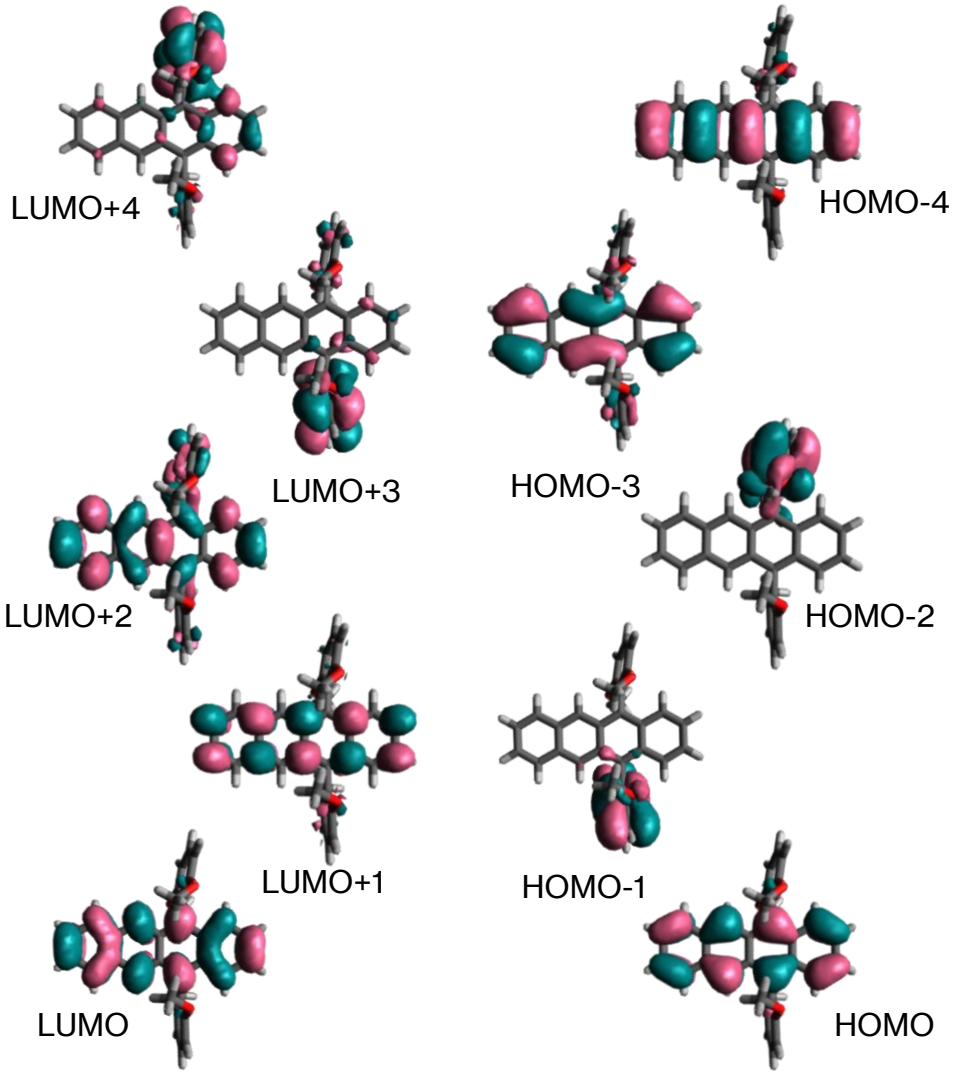

Figure S4. Frontier molecular orbitals of **Encap-T**.

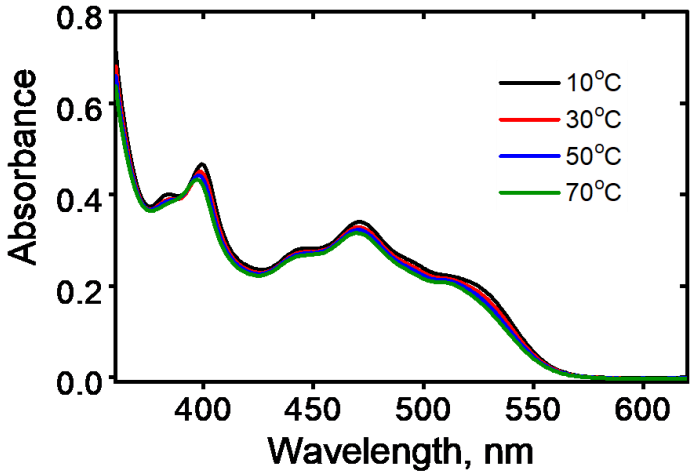

Figure S5: Temperature-dependent UV–vis absorption spectra of **Encap-TAT** in toluene (10–70 °C). The unchanged spectral profile across this range rules out aggregation under these conditions.

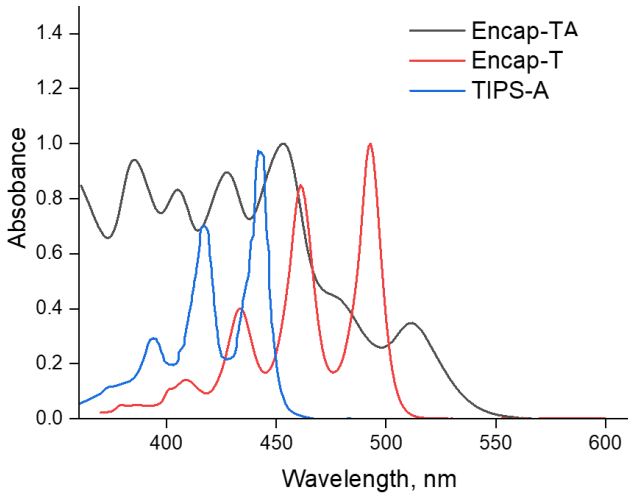

Figure S6: Normalised absorption spectra of **Encap-TA**, **Encap-T** and **TIPS-A** in toluene at room temperature.

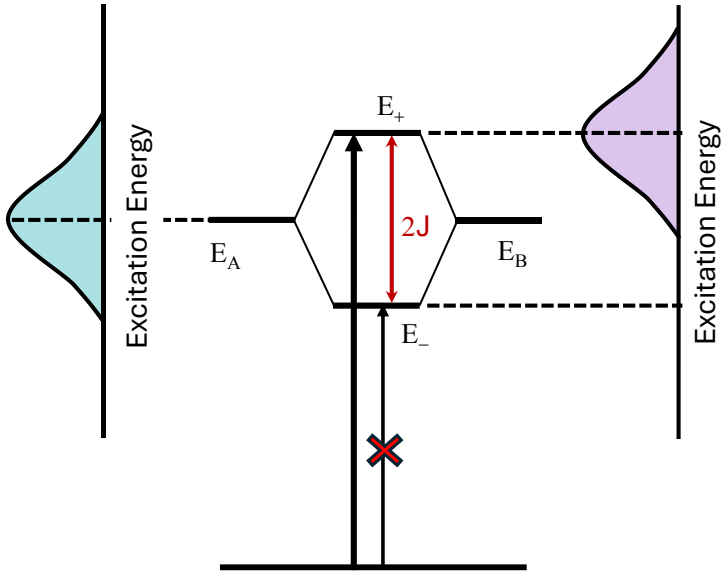

Figure S7: Schematic representation of excitonic coupling in a dimer system. Two monomers with identical excitation energies (blue spectrum on left side) interact via Coulombic coupling, resulting in exciton splitting into two delocalized states separated by 2J. Due to the symmetric (bright) and antisymmetric (dark) nature of the resulting eigenstates, only the higher-energy state is optically allowed (indicated by the vertical arrow), while the lower-energy dark state is forbidden by symmetry (marked with a red X).

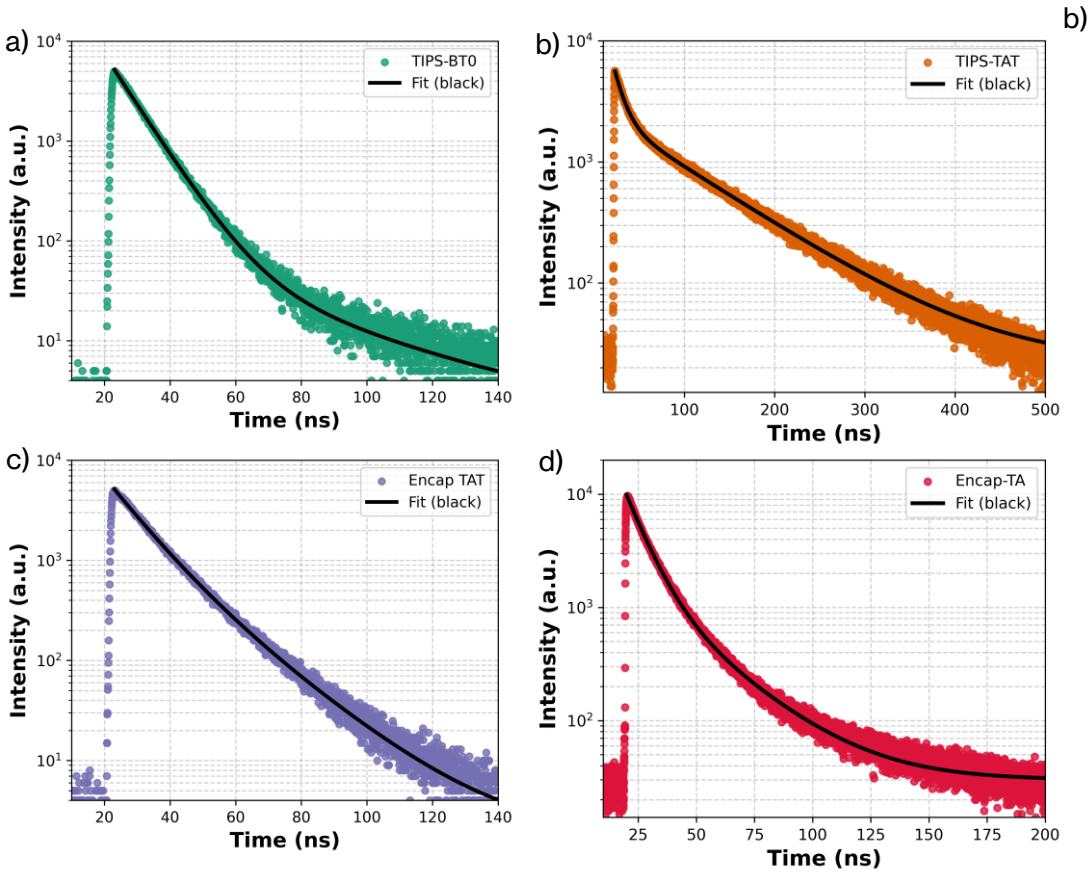

Figure S8: Time-resolved fluorescence decay profiles of **TIPS-BT0** (a), **TIPS-TAT** (b), **Encap-TAT** (c), and **Encap-TA** (d) in dilute toluene solution (λ_{exci}=470 nm, collection at 505 nm)

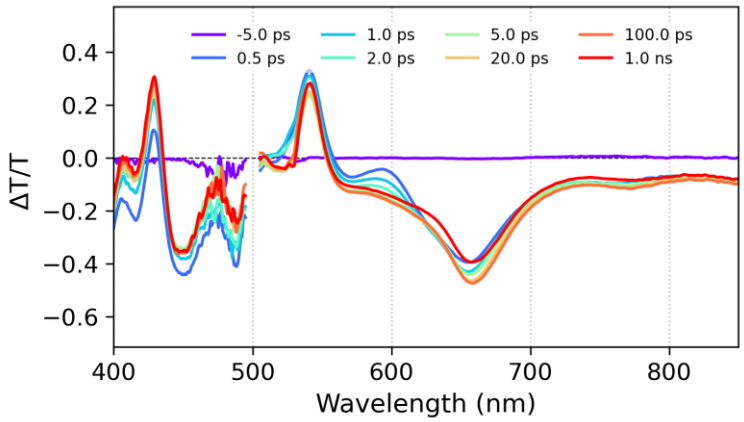

Figure S9: Femtosecond transient absorption spectra of **TIPS-BT0** in toluene following 470 nm excitation, capturing the ensuing excited-state dynamics.

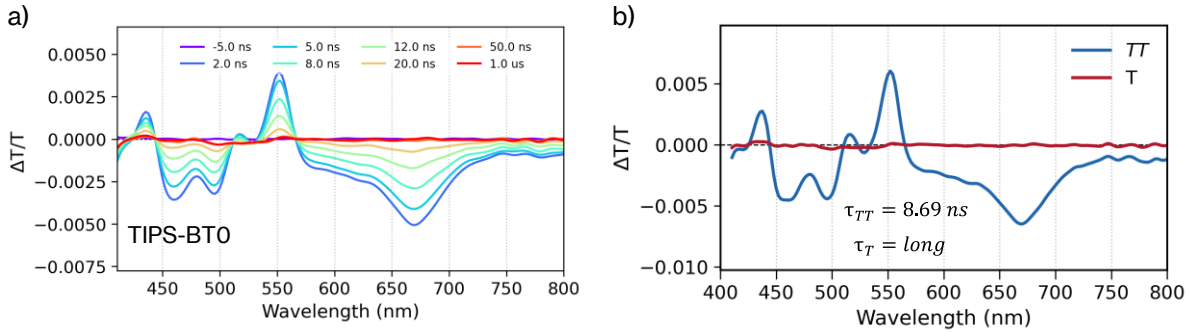

Figure S10: Selected femtosecond transient absorption spectra of **TIPS-BT0** at representative delays (left) spectra and evolution-associated difference spectra (EADS) profiles from global analysis using a sequential model.

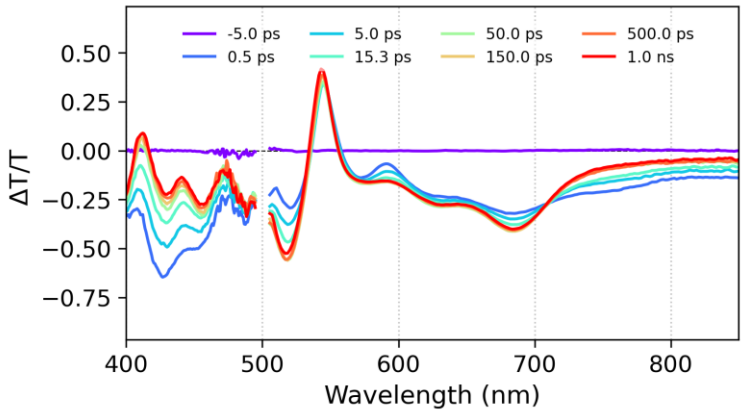

Figure S11: Femtosecond transient absorption spectra of **TIPS-TAT** in toluene following 470 nm excitation, capturing the ensuing excited-state dynamics.

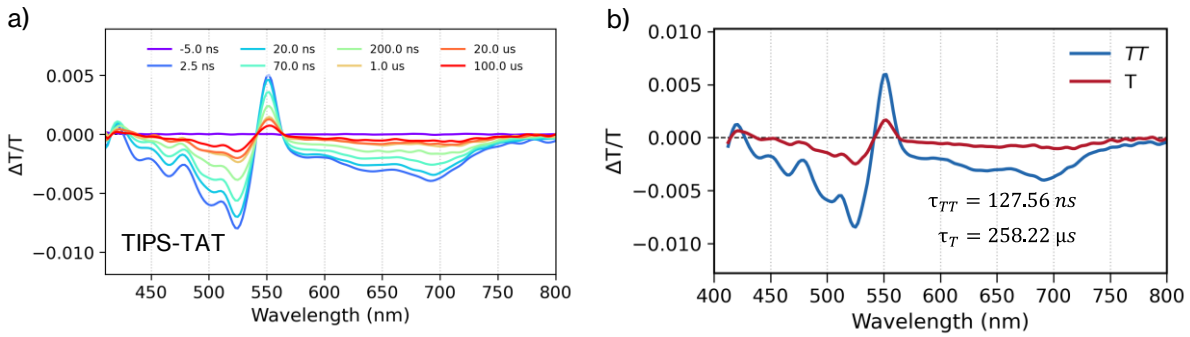

Figure S12: Selected femtosecond transient absorption spectra of **TIPS-TAT** at representative delays (left) spectra and evolution-associated difference spectra (EADS) profiles from global analysis using a sequential model.

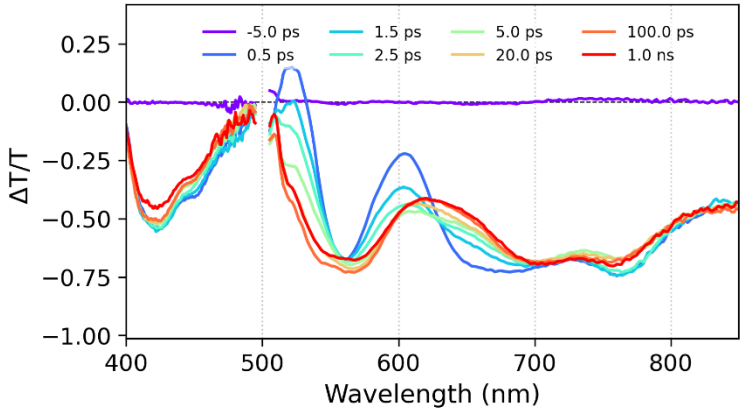

Figure S13: Femtosecond transient absorption spectra of **Encap-TAT** in toluene following 470 nm excitation, capturing the ensuing excited-state dynamics.

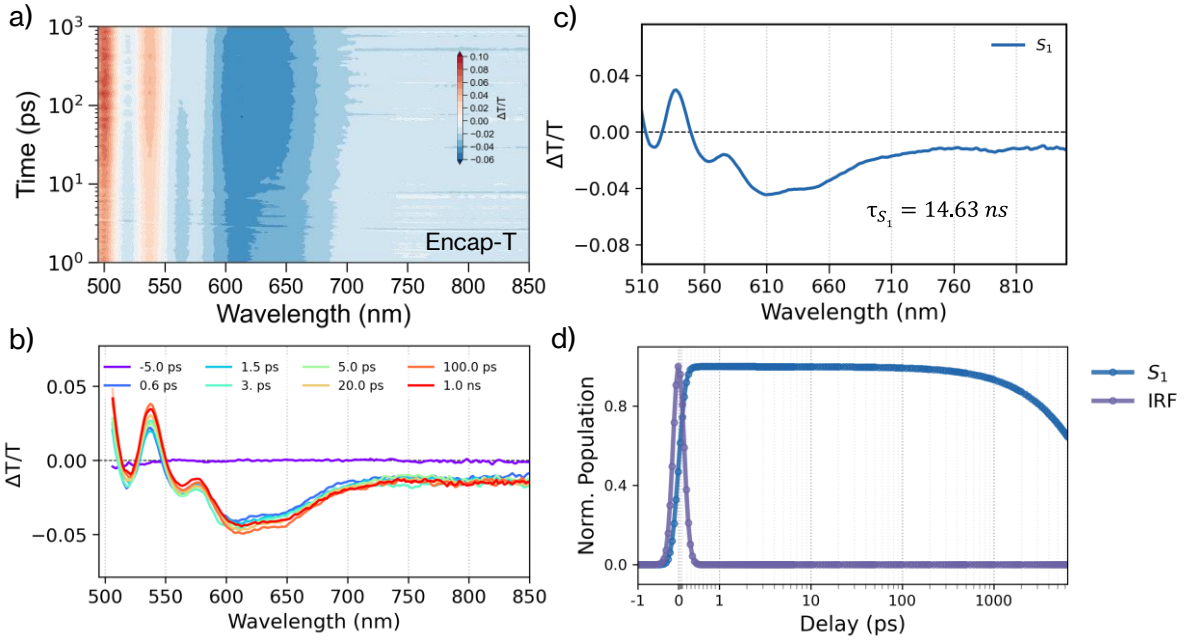

Figure S14: Femtosecond transient absorption (fsTA) of **Encap-T** in toluene following 470 nm excitation. (a) Contour map (ΔT/T vs wavelength and delay). (b) Selected spectra at representative delays. (c) Evolution-associated difference spectra (EADS). (d) Kinetic population profiles from global analysis using a sequential model.

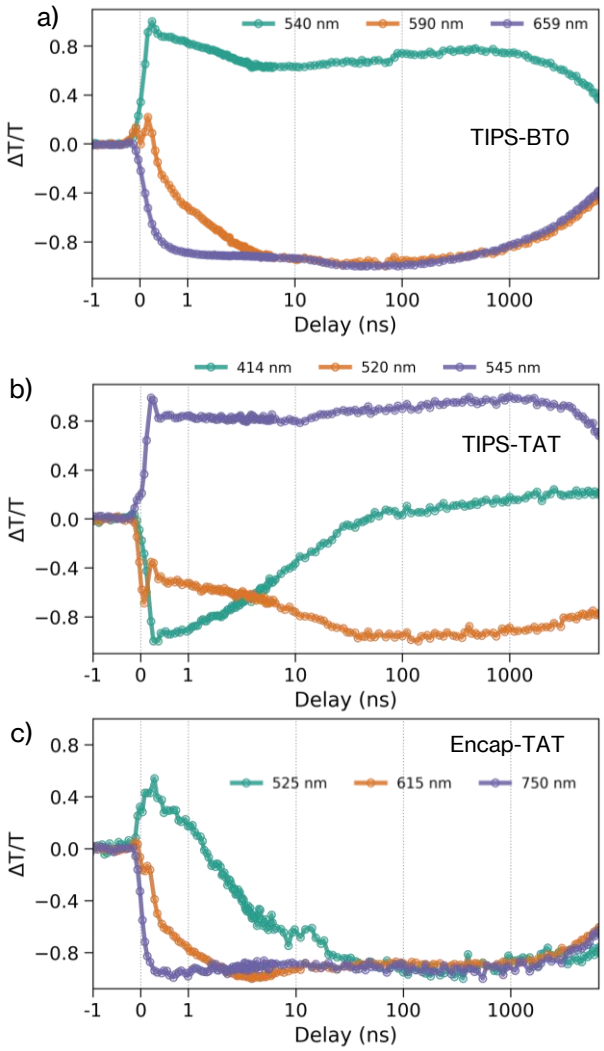

Figure S15: Selected kinetics traces from femtosecond transient absorption data of **TIPS-BT0** (a), **TIPS-TAT**(b) and **Encap-TAT** (c) in toluene following 530 nm excitation.

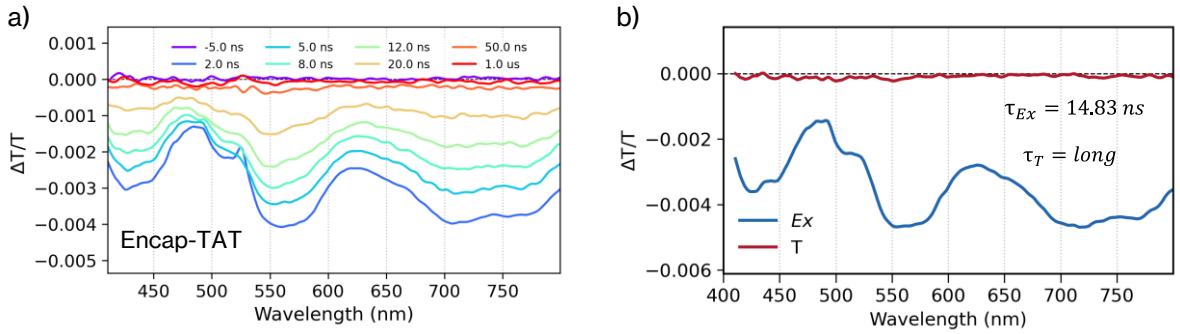

Figure S16: Selected femtosecond transient absorption spectra of **Encap-TAT** at representative delays (left) spectra and evolution-associated difference spectra (EADS) profiles from global analysis using a sequential model.

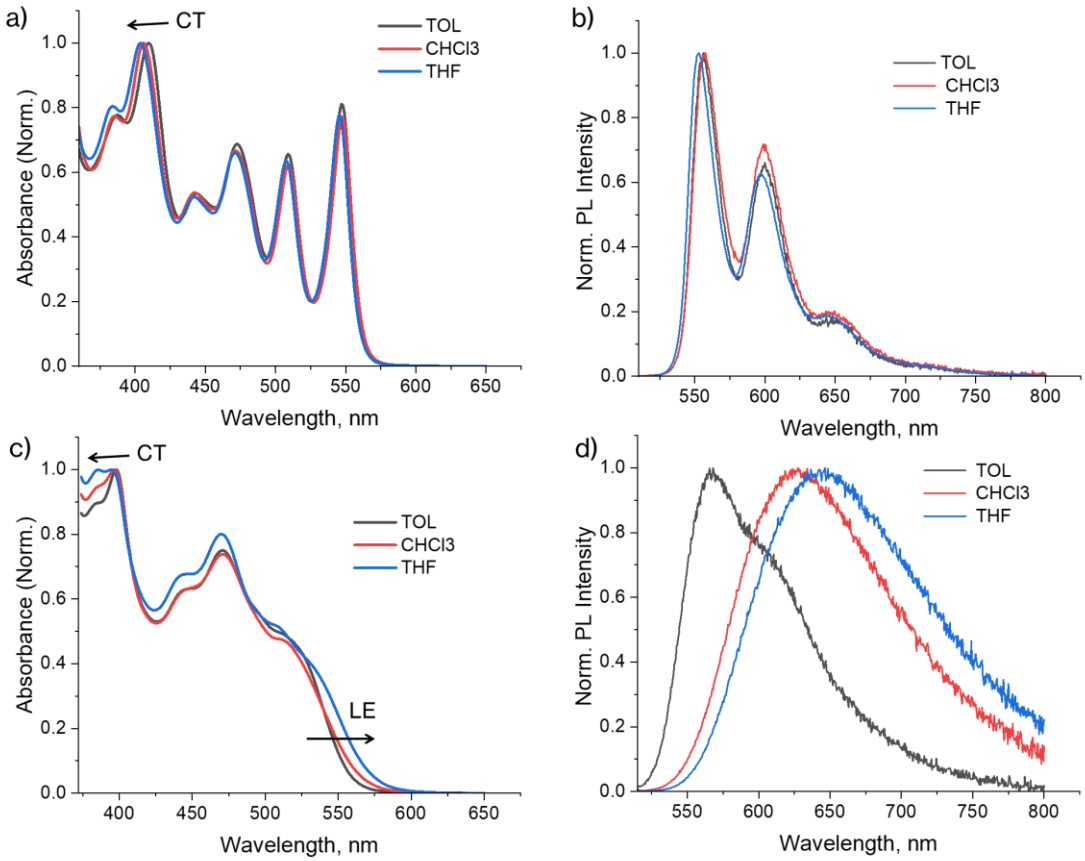

Figure S17: Steady state absorption and PL spectra of **TIPS-TAT** (a and b) and **Encap-TAT** (c and d) recorded in solvents spanning low to moderate polarity: toluene (TOL, ε_r = 2.38), chloroform ($CHCl_3$, ε_r = 4.81), and tetrahydrofuran (THF, ε_r = 7.58). The dielectric constants (ε_r) are reported at ~20–25 °C

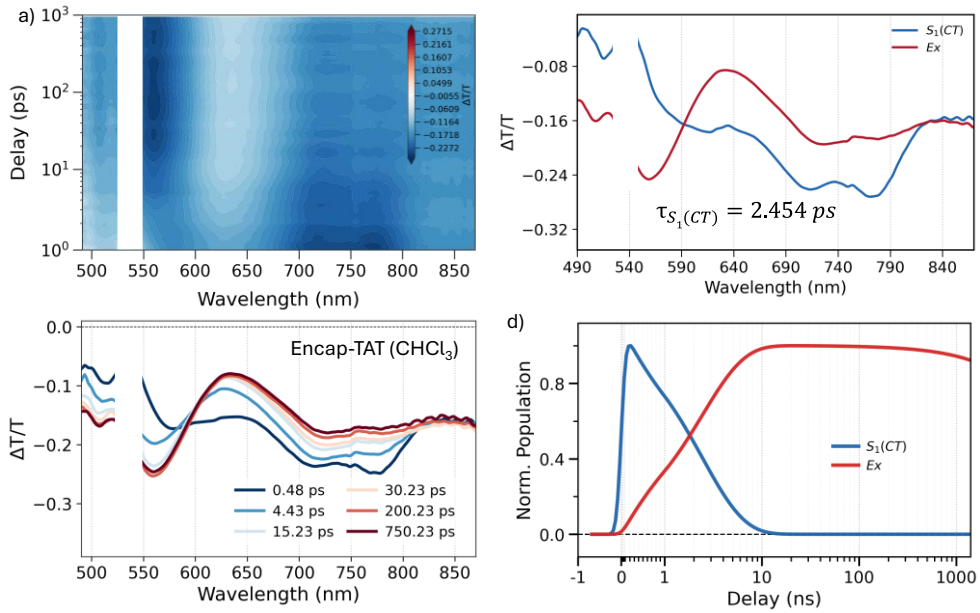

Figure S18: Femtosecond transient absorption (fsTA) of **Encap-TAT** in chloroform following 530 nm excitation. (a) Contour map (ΔT/T vs wavelength and delay). (b) Selected spectra at representative delays. (c) Evolution-associated difference spectra (EADS). (d) Kinetic population profiles from global analysis using a sequential model.

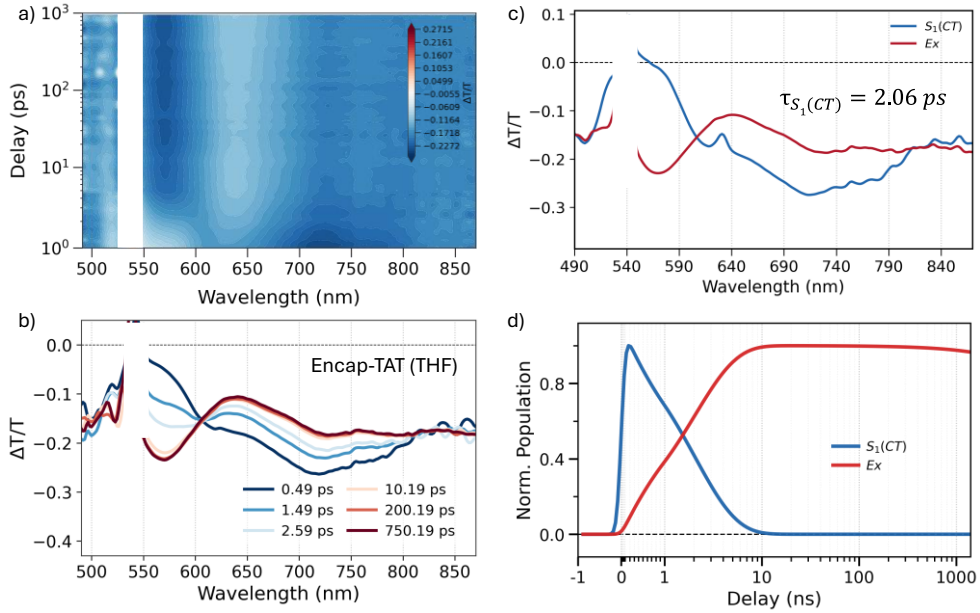

Figure S19: Femtosecond transient absorption (fsTA) of **Encap-TAT** in tetrahydrofuran following 530 nm excitation. (a) Contour map (ΔT/T vs wavelength and delay). (b) Selected spectra at representative delays. (c) Evolution-associated difference spectra (EADS). (d) Kinetic population profiles from global analysis using a sequential model.

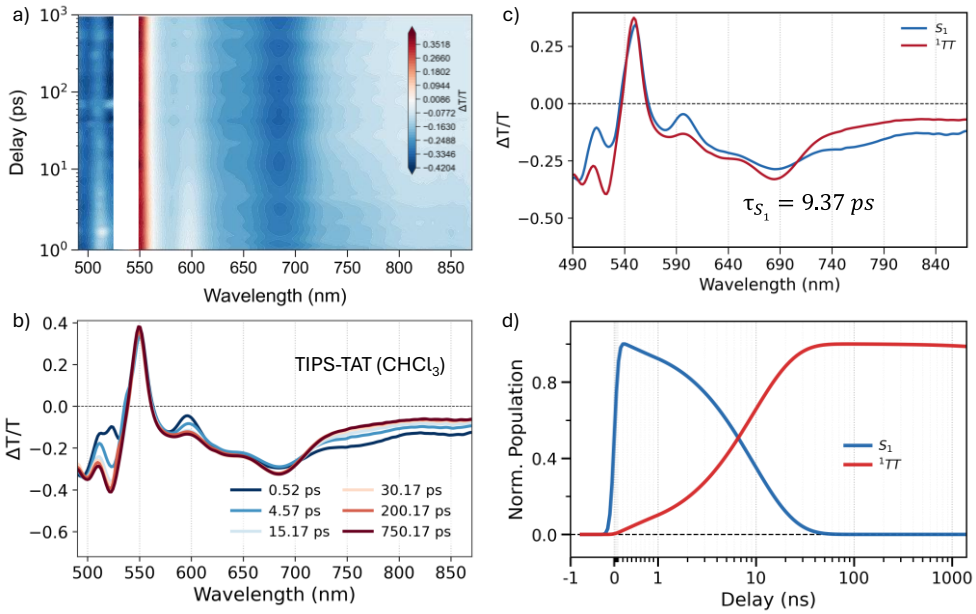

Figure S20: Femtosecond transient absorption (fsTA) of **TIPS-TAT** in chloroform following 530 nm excitation. (a) Contour map (ΔT/T vs wavelength and delay). (b) Selected spectra at representative delays. (c) Evolution-associated difference spectra (EADS). (d) Kinetic population profiles from global analysis using a sequential model.

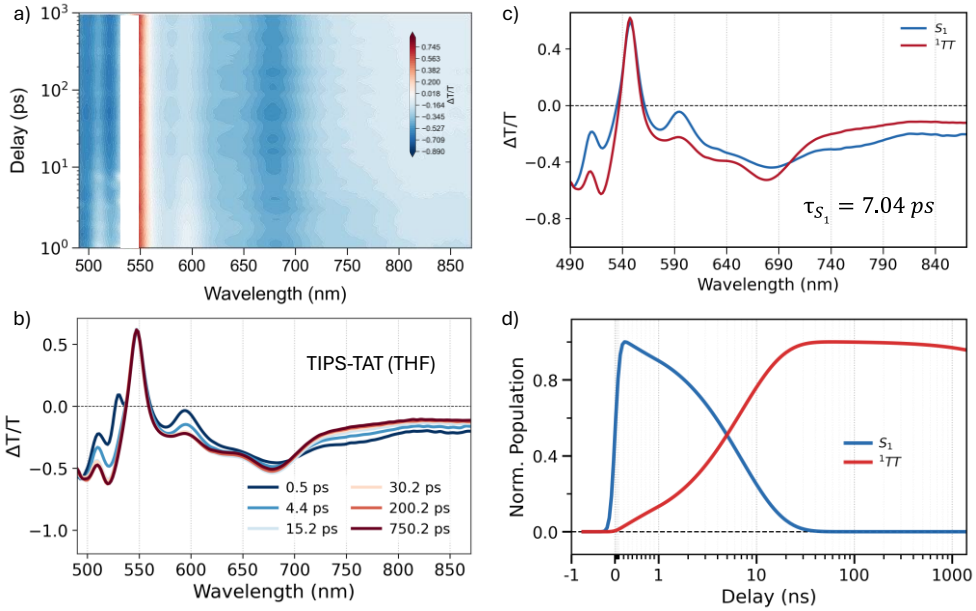

Figure S21: Femtosecond transient absorption (fsTA) of **TIPS-TAT** in Tetrahydrofuran following 530 nm excitation. (a) Contour map (ΔT/T vs wavelength and delay). (b) Selected spectra at representative delays. (c) Evolution-associated difference spectra (EADS). (d) Kinetic population profiles from global analysis using a sequential model.

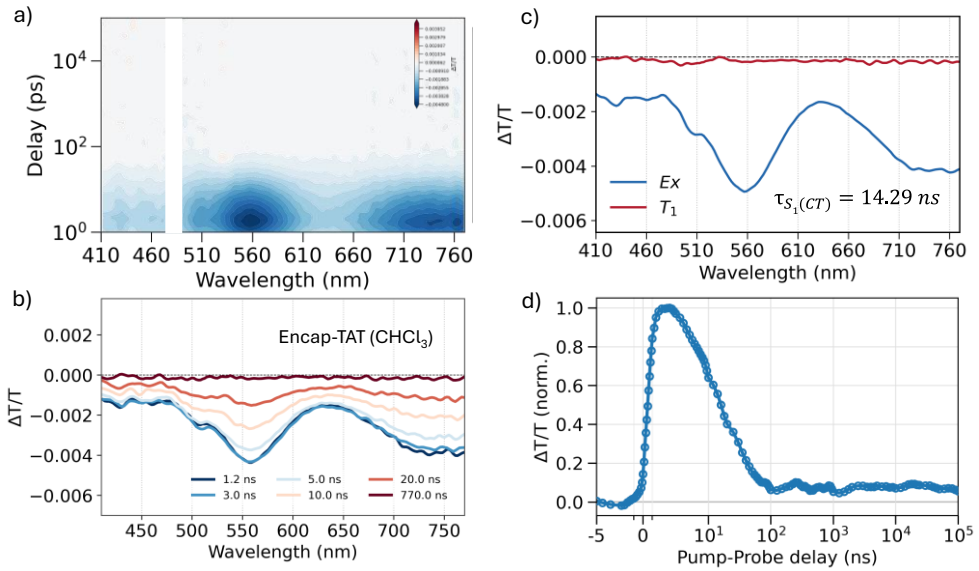

Figure S22: Nanosecond transient absorption (nsTA) of **Encap-TAT** in chloroform following 532 nm excitation. (a) Contour map (ΔT/T vs wavelength and delay). (b) Selected spectra at representative delays. (c) Evolution-associated difference spectra (EADS) from global analysis with a sequential model. (d) Kinetic profiles **Encap-TAT** at the 510 nm.

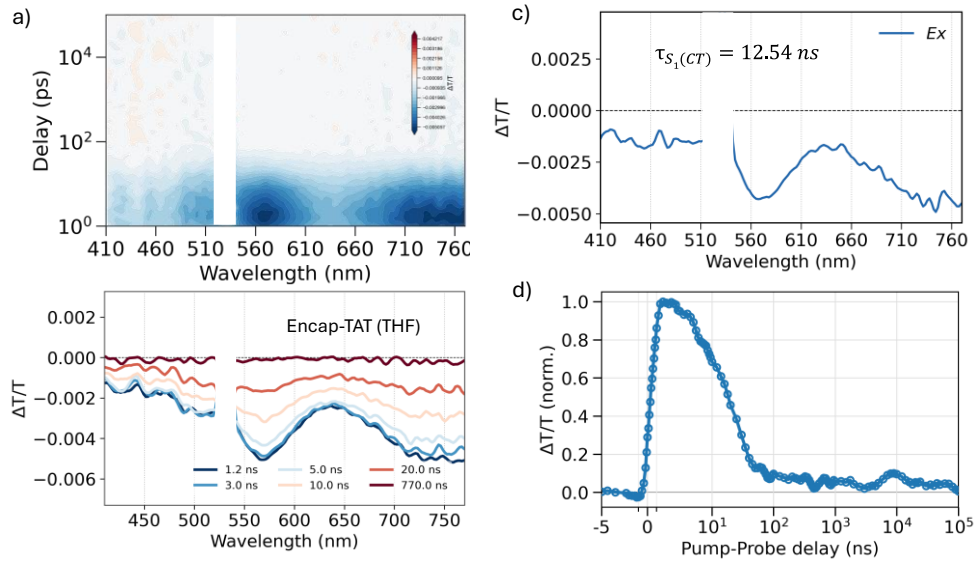

Figure S23: Nanosecond transient absorption (nsTA) of **Encap-TAT** in tetrahydrofuran following 532 nm excitation. (a) Contour map (ΔT/T vs wavelength and delay). (b) Selected spectra at representative delays. (c) Evolution-associated difference spectra (EADS) from global analysis with a sequential model. (d) Kinetic profiles **Encap-TAT** at the 510 nm.

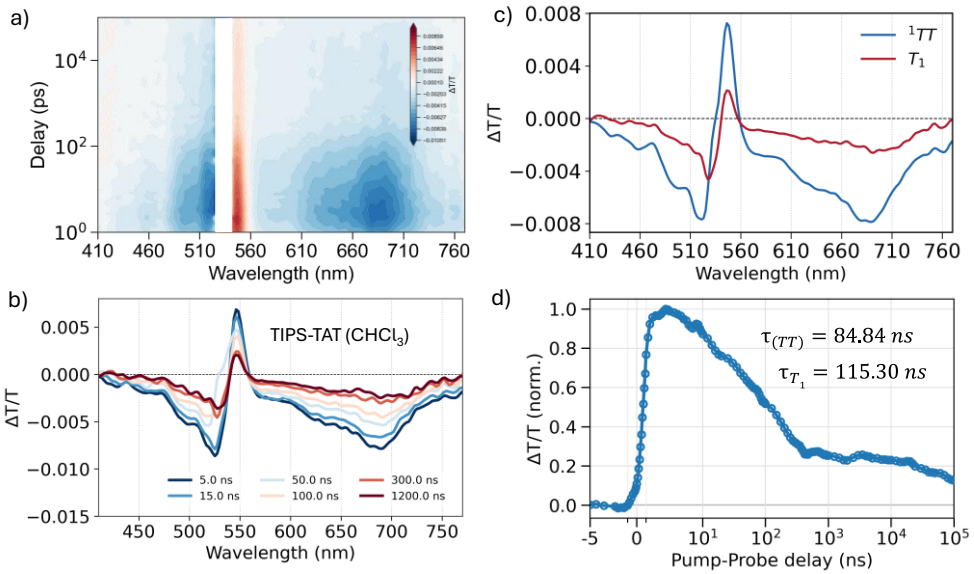

Figure S24: Nanosecond transient absorption (nsTA) of **TIPS-TAT** in chloroform following 532 nm excitation. (a) Contour map (ΔT/T vs wavelength and delay). (b) Selected spectra at representative delays. (c) Evolution-associated difference spectra (EADS) from global analysis with a sequential model. (d) Kinetic profiles **TIPS-TAT** at the 680 nm.

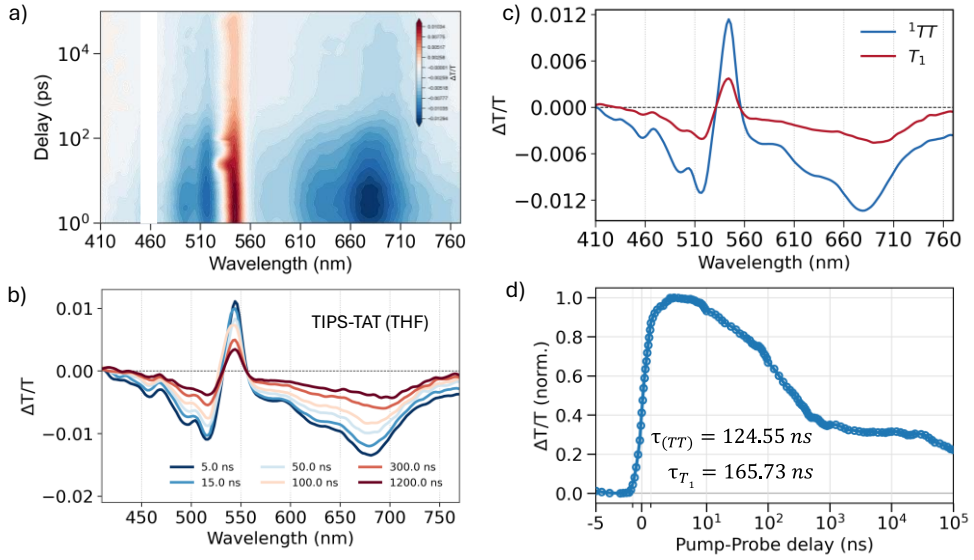

Figure S25: Nanosecond transient absorption (nsTA) of **TIPS-TAT** in tetrahydrofuran following 532 nm excitation. (a) Contour map (ΔT/T vs wavelength and delay). (b) Selected spectra at representative delays. (c) Evolution-associated difference spectra (EADS) from global analysis with a sequential model. (d) Kinetic profiles **TIPS-TAT** at the 680 nm.

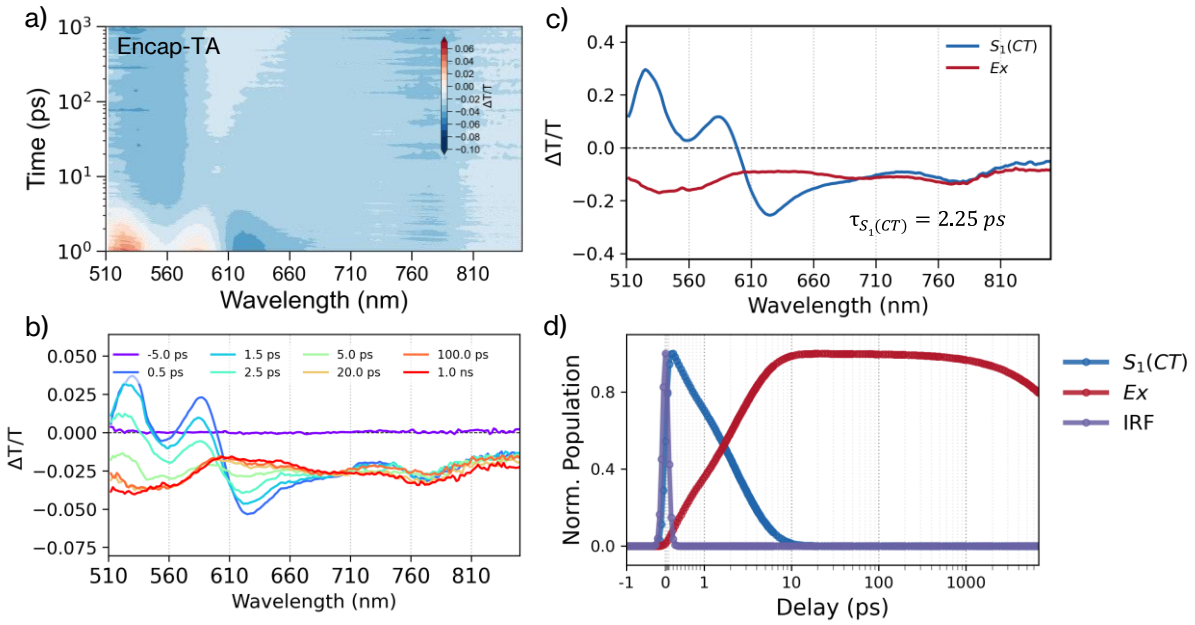

Figure S26: Femtosecond transient absorption (fsTA) of **Encap-TA** in toluene following 530 nm excitation. (a) Contour map (ΔT/T vs wavelength and delay). (b) Selected spectra at representative delays. (c) Evolution-associated difference spectra (EADS). (d) Kinetic population profiles from global analysis using a sequential model.

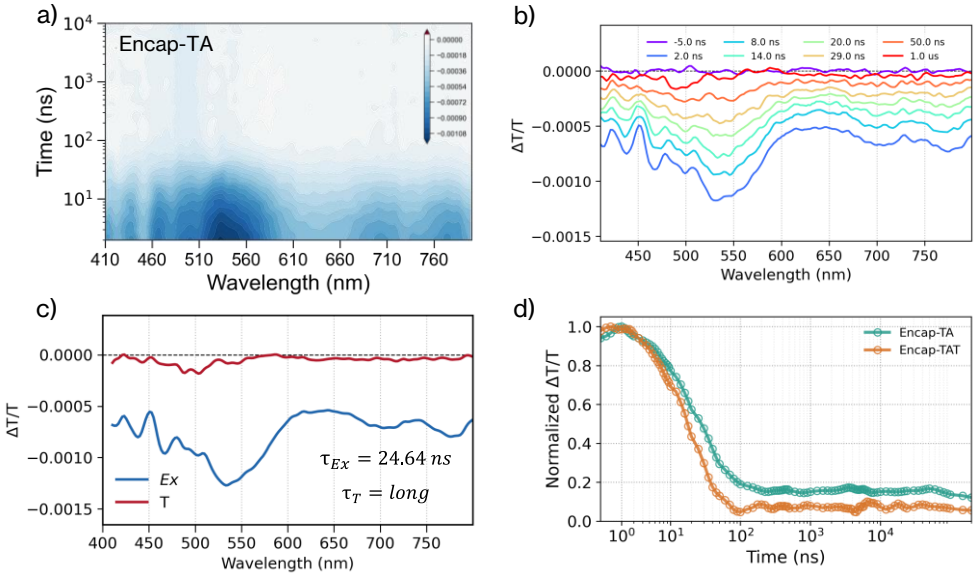

Figure S27: Nanosecond transient absorption (nsTA) of **Encap-TA** in toluene following 532 nm excitation. (a) Contour map (ΔT/T vs wavelength and delay). (b) Selected spectra at representative delays. (c) Evolution-associated difference spectra (EADS) from global analysis with a sequential model. (d) Comparison of Kinetic profiles **Encap-TAT** and **Encap-TA** in the 470-500 nm region.

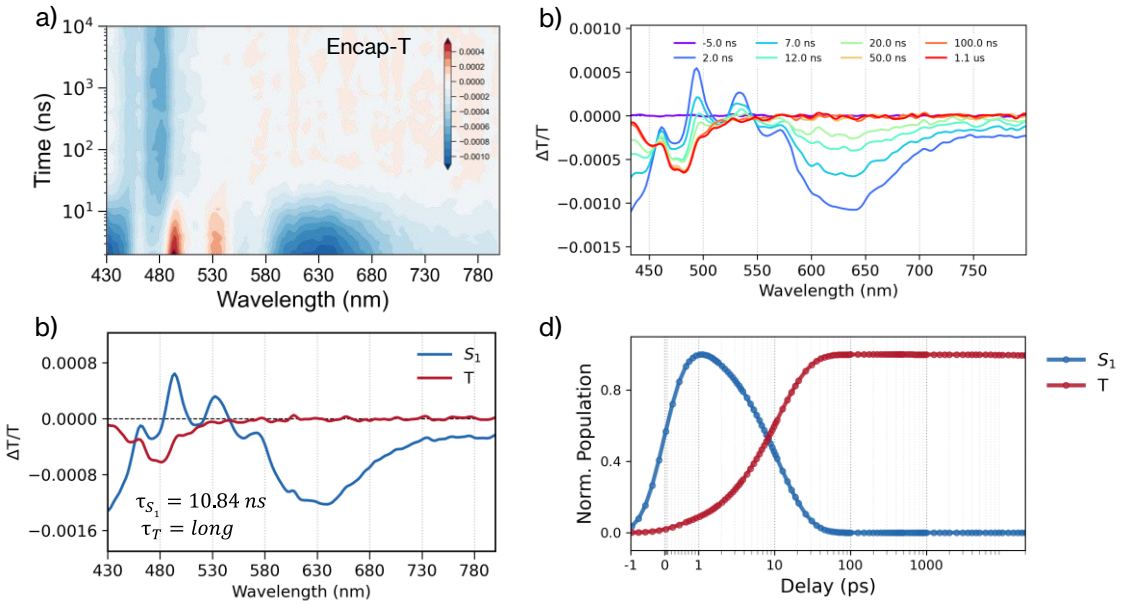

Figure S28: Nanosecond transient absorption (nsTA) of **Encap-T** in toluene following 400 nm excitation. (a) Contour map (ΔT/T vs wavelength and delay). (b) Selected spectra at representative delays. (c) Evolution-associated difference spectra (EADS). (d) Kinetic population profiles from global analysis using a sequential model.

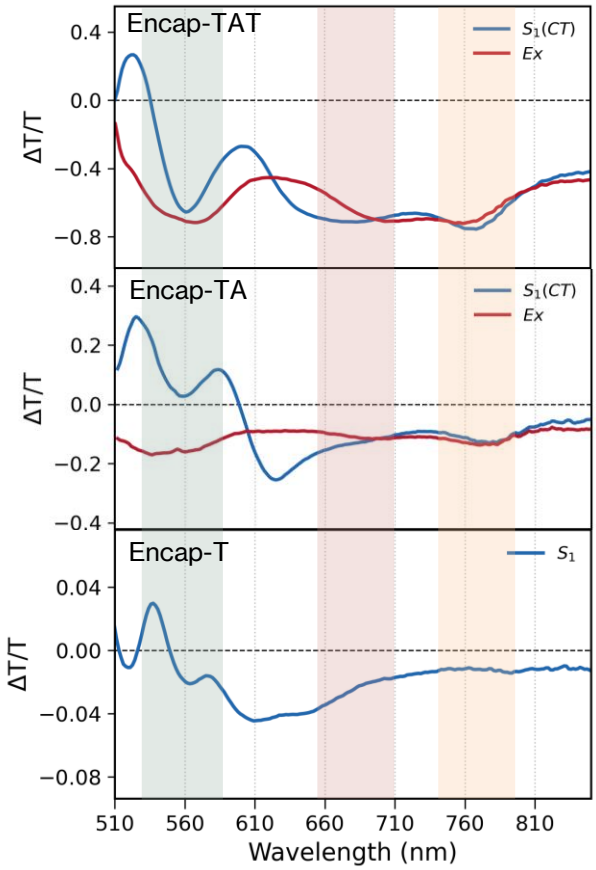

Figure S29: Comparison of Evolution-associated difference spectra (EADS) of **Encap-TAT** (a). **Encap-TA** (b) and **Encap-T** (c) obtained global analysis.

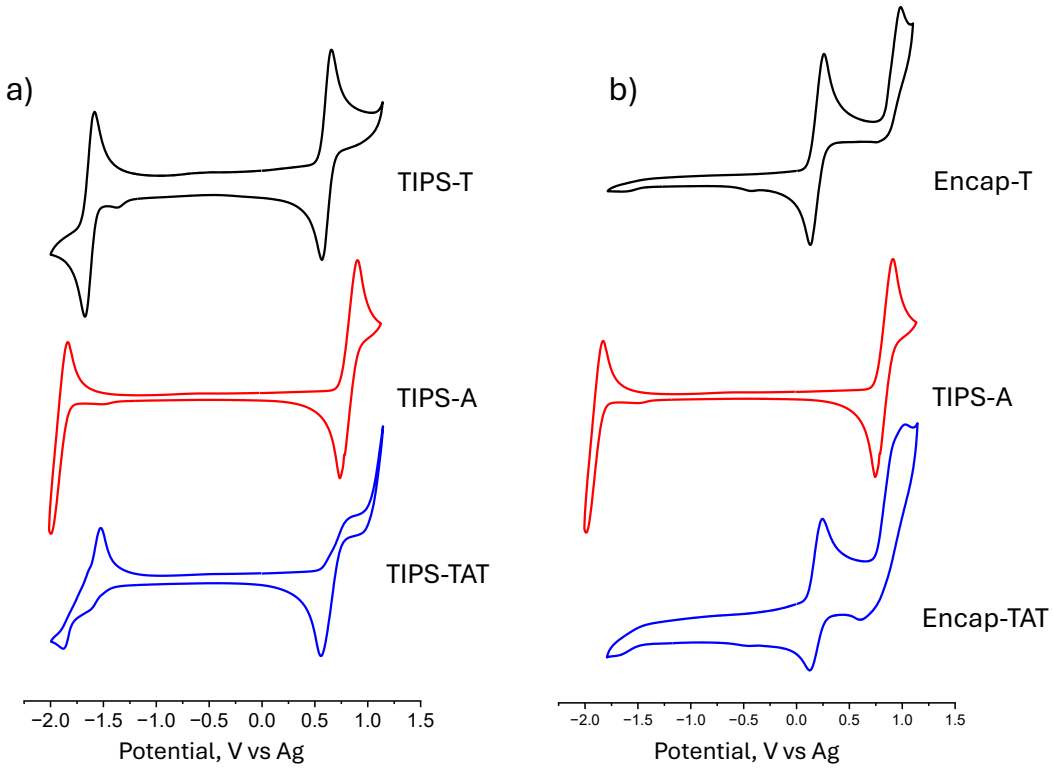

Figure S30. Cyclic voltammograms of **TIPS-T**, **TIPS-A**, **TIPS-TAT**, **Encap-T** and **Encap-TAT**.

Section 4: Solvent Polarity Dependence of LE–CT Mixing and Excited-State Branching

To assess how the local dielectric environment modulates exciton–CT hybridisation and the resulting excited-state branching, we measured solvent-dependent femtosecond and nanosecond transient absorption (TA) for representative systems in the strong (**Encap-TAT**) and weak/moderate (**TIPS-TAT**) FE–CT mixing limits (Figures S18–S25), complemented by solvent-dependent steady-state emission. Increasing solvent polarity stabilises charge-transfer (CT) configurations relative to locally excited (LE) states, reducing the LE–CT energy gap. Depending on the coupling regime, this stabilization can either (i) drive relaxation into a CT-rich exciplex-like minimum (strong mixing) or (ii) enhance CT-mediated superexchange into the correlated triplet-pair manifold (^{1}TT) without forming a trapped CT minimum (weak/moderate mixing).

Strong FE–CT mixing: exciplex-forming regime (Encap-TAT)

In the strong-mixing limit, dielectric stabilisation lowers the CT surface and increases CT character in the lowest adiabatic excited state, favouring rapid relaxation into a CT-rich intramolecular exciplex-like state (Ex). The fsTA data for **Encap-TAT** in chloroform and THF (Figures S18 and S19, respectively) show that the early-time spectral evolution remains qualitatively similar across solvents, but the kinetics accelerate with increasing polarity. Global analysis using a sequential model yields a systematic decrease in the Ex-formation time constant from 2.95 ps (toluene) to 2.45 ps ($CHCl_3$) and 2.06 ps (THF), consistent with a larger driving force for structural/solvent reorganisation into a CT-stabilised minimum. In parallel, the steady-state emission exhibits a pronounced red shift with increasing polarity (Figure S17), supporting a more dipolar emissive state and reinforcing the assignment of Ex as a CT-enriched relaxed minimum rather than a tetracene-localised multiexciton product.

Nanosecond TA further supports this interpretation. The nsTA datasets for **Encap-TAT** in $CHCl_3$ and THF are shown in Figures S22 and S23. Although the long-lived spectra display broadly triplet-like PIA features, the dominant decay channel is ground-state recovery rather than accumulation of persistent triplets. Importantly, the Ex-lifetime shortens systematically with increasing dielectric constant, decreasing from 16.9 ns (TOL) to 14.29 ns ($CHCl_3$) and 12.54 ns (THF). This polarity-accelerated decay is consistent with stabilisation of Ex-state minimum that enhances nonradiative deactivation as the CT character increases, providing a solvent-dependent diagnostic that supports the exciplex-like assignment.

Weak/moderate FE–CT mixing: superexchange iSF regime (TIPS-TAT)

In the weak/moderate mixing limit, the CT configuration primarily acts as a virtual intermediate that mediates LE → ^{1}TT via superexchange rather than forming a Ex-state minimum. Stabilising the CT configuration with increasing polarity reduces LE–CT detuning and is therefore expected to increase the effectiveness of the superexchange pathway, accelerating ^{1}TT formation. Consistent with this expectation, the fsTA datasets for TIPS-TAT in chloroform and THF (Figures S20 and S21) show a systematic acceleration of singlet fission with solvent polarity: τ_{SF} = 11.2 ps (TOL), 9.37 ps ($CHCl_3$), and 7.04 ps (THF). Notably, the early-time spectra do not evolve toward the broad, featureless Ex-like signatures observed for **Encap-TAT**; instead, the spectral evolution remains consistent with formation of a tetracene-localised correlated triplet-pair manifold.

In the nanosecond regime, the nsTA datasets for **TIPS-TAT** in $CHCl_3$ and THF (Figures S24 and S25) show that the long-lived ^{1}TT-derived triplet signal exhibits a lifetime comparable to that observed in toluene within experimental uncertainty. Thus, while solvent polarity influences the rate of ^{1}TT formation (consistent with enhanced superexchange), it does not strongly promote polarity-driven quenching or rapid ground-state recovery in the SF-active system. The persistence of the ^{1}TT/triplet manifold enables continued evolution toward long-lived free triplets rather than diversion into an exciplex-like trap.

Overall, the solvent-dependent fsTA and nsTA results provide a straightforward mechanistic discriminator between the strong- and weak/moderate-mixing limits (Figure S30). Polarity stabilises CT configurations in both cases, but the outcome depends on coupling strength and energetic alignment. In strongly mixed systems (**Encap-TAT**),

stabilised CT surfaces promote rapid relaxation into a exciplex-like minimum and accelerate its decay back to the ground state. In weak/moderate mixing systems (**TIPS-TAT**), stabilised CT primarily enhances CT-assisted superexchange and accelerates ^{1}TT formation without stabilising a trapped exciplex minimum on the measured timescales. These trends strengthen the assignments of the observed transients and directly support the central conclusion that excessive bridge-resonant LE–CT hybridisation suppresses iSF by funnelling population into an exciplex-like trap.

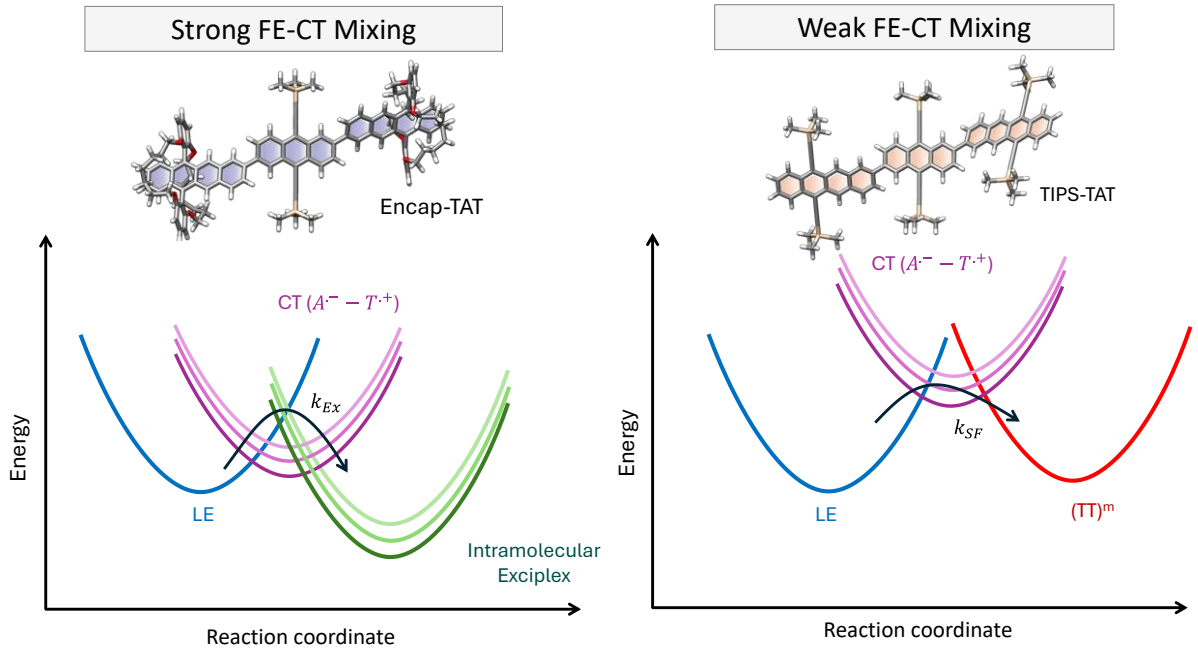

Figure S31. Schematic potential-energy surfaces illustrating how solvent polarity modulates excited-state branching in the strong and weak FE–CT mixing limits. Left: Strong FE–CT mixing, where dielectric stabilisation lowers the CT surface (purple) relative to the LE surface (blue), increasing adiabatic CT character and promoting ultrafast relaxation into an intramolecular exciplex-like minimum (green). The observed Ex formation accelerates with polarity, accompanied by red-shifted emission consistent with a more dipolar emissive state. Right: Weak FE–CT mixing, where the CT configuration acts primarily as a virtual intermediate that mediates LE → ^{1}TT (red) via superexchange. Increasing solvent polarity stabilises CT and reduces LE–CT detuning, leading to faster ^{1}TT formation without stabilising a trapped exciplex minimum.

Section 5: Syntheses and Characterisation

3,5-Dimethoxyphrnyl triflate,[14] Bis(BPin)-TIPS-anthracene[15] and BPin-TIPS-anthracene[16] were synthesised according to literature procedures. We note that we found Bis(BPin)-TIPS-anthracene to be bench stable, in contrast to a previous report.[15]

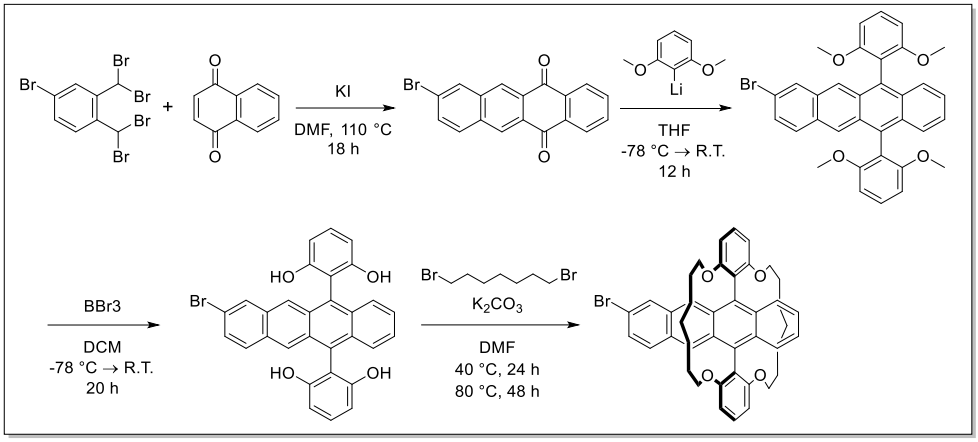

Scheme 1. Synthesis of the Encapsulated Bromo Tetracene (Encap-Tet-Br)

Synthesis of 8-bromo-5,12-tetracenequinone

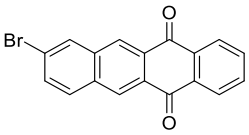

To a 250 mL flask under argon, 1,4-naphthoquinone (1.60 g, 10.1170 mmol), α,α,α',α',4-Pentabromo-o-xylene (5.00 g, 9.9870 mmol), potassium iodide (6.50 g, 39.1566 mmol) and anhydrous DMF (120 mL) were added and the mixture was heated to 110 ºC for 18 h. Next, the reaction mixture was cooled to room temperature and poured into stirring MeOH (200 mL). The product was collected by filtration, washed with water (100 mL). The shiny yellow-golden solids were then sonicated and filtered from both MeOH (1 x 50 mL) and chloroform (1 x 50 mL) and collected to afford pure product (1.7854 g, 5.2952 mmol, 53%).

The product has only limited solubility in most organic solvents, however ^{1}H NMR and Mass spec confirmed product formation. The product was used in the next step without further purification.

^{1}H NMR (400 MHz, $CDCl_3$) δ 8.81 (d, J = 27.1 Hz, 2H), 8.40 (dd, J = 5.8, 3.3 Hz, 2H), 8.28 (s, 1H), 7.98 (d, J = 8.7 Hz, 1H), 7.85 (dd, J = 5.8, 3.3 Hz, 2H), 7.78 (dd, J = 8.7, 1.8 Hz, 1H). **HRMS** (ASAP-TOF): Calculated for $C_{18}H_{10}BrO_2^+$: 336.9853. Found m/z 336.9864 $[M+H]^+$.

Synthesis of 8-bromo-5,12-bis(2,6-dimethoxyphenyl)tetracene (Br-Tet-OMe)

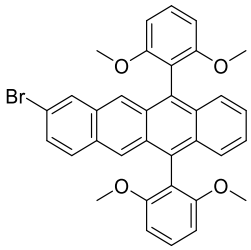

In a dry flask under argon at 0 ºC, n-BuLi (10.56 mL, 1.6 M, 16.8960 mmol) was added dropwise to a solution of 1,3-dimethoxybenzene (2.34 mL, 17.8684 mmol) and dry TMEDA (2.67 mL, 17.8077 mmol) in anhydrous THF (30 mL). Next, the reaction was warmed to room temperature and left stirring for 30 minutes. Next, the mixture was cooled to -78 ºC, after which solid Br-Tet-Quinone (1.5 g, 4.4488 mmol) was added in one portion. The reaction was left to warm to room temperature and stirred for 12 h at room temperature. The reaction was quenched using saturated NH_4Cl solution and it was extracted with DCM (3 x). The combined organic layer was dried over $MgSO_4$, filtered and concentrated in vacuo. Next, the residue was re-dissolved in regular THF (~150 mL) and a solution of $SnCl_2$ x $2H_2O$ (4.2 g) in THF (180 mL) and glacial AcOH (30 mL). The reaction was left stirring for 3 h at room temperature. The resulting mixture was concentrated in vacuo (use toluene to co-evaporate AcOH). The residue was then dissolved in DCM (~200 mL) and washed with 1M HCl (2 x 100 mL). The aqueous layer was extracted with DCM (~100 mL) and the combined organic layer was dried over $MgSO_4$, filtered and concentrated in vacuo. The resulting residue was purified via silica column chromatography (stepwise column; starting with 100% hexane, then 15% DCM to remove leftover 1,3-dimethoxybenzene and finally 25 to 35% DCM to elute the product). The product fractions were concentrated in vacuo, after which the solids were sonicated in hexane (and a tiny amount of DCM) and collected by filtration to afford the product as a bright yellow solid (1.6097 g, 2.7778 mmol, 62%).

^{1}H NMR (700 MHz, $CDCl_3$) δ 8.22 (s, 1H), 8.15 (s, 1H), 7.98 (s, 1H), 7.66 (d, J = 9.1 Hz, 1H), 7.58 (dt, J = 16.8, 7.9 Hz, 4H), 7.25 (s, 1H), 7.24 – 7.20 (m, 2H), 6.89 – 6.84 (m, 4H). **HRMS** (ASAP-TOF): Calculated for $C_{34}H_{28}O_4Br^+$: 579.1171. Found m/z 579.1161 $[M+H]^+$.

Synthesis of 8-bromo-5,12-bis(resorcinol)tetracene (Br-Tet-OH)

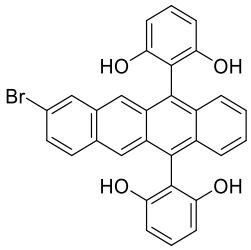

In a dry flask under argon at -78 ºC, BBr_3 (14 mL, 1.0 M, 14 mmol) was added dropwise to a solution of Br-Tet-OMe (1 g, 1.7257 mmol) in dry DCM (100 mL). The reaction was allowed to warm to room temperature and was stirred for 20 h (monitored by NMR). Next, the reaction mixture was poured into a stirring saturated $NaHCO_3$ solution (~200 mL) and the DCM layer was separated. Next, it was extracted with EtOAc (2 x 150 mL). The combined organic layers were concentrated in vacuo and purified via silica column chromatography (stepwise column; starting with 100% hexane,

then going gradually to 100% DCM and finally 1, 2, 5 and 10% EtOAc). The product was eluted with 5-10% EtOAc in DCM. The product fractions were concentrated in vacuo, after which the solids were sonicated in hexane (and a tiny amount of DCM) and collected by filtration to afford the product as an orange solid (580.5 mg, 1.1091 mmol, 95%).

^{1}H NMR (700 MHz, DMSO) δ 9.01 (s, 4H), 8.29 (s, 2H), 7.89 – 7.81 (m, 2H), 7.64 – 7.56 (m, 2H), 7.29 (dd, J = 35.9, 7.1 Hz, 4H), 7.24 (t, J = 8.2 Hz, 2H), 6.65 (d, J = 8.1 Hz, 4H). **HRMS** (ASAP-TOF): Calculated for $C_{30}H_{20}O_4Br^+$: 523.0545. Found m/z 523.0544 $[M+H]^+$.

Synthesis of Encapsulated Bromo Tetracene (Encap-Tet-Br)

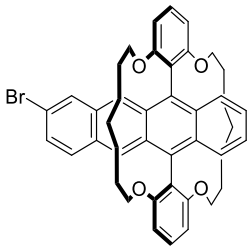

Under argon, 1,7-dibromoheptane (0.19 mL, 1.1120 mmol) was added to a mixture of T-OH (280 mg, 0.5350 mmol) and K_2CO_3 (370 mg, 2.6771 mmol) in dry DMF (105 mL) and the reaction mixture was heated to 40 ºC for 24 h and 80 ºC for 48 h. Next, it was concentrated in vacuo and the crude product was purified via silica column chromatography using 30% DCM in hexane. The product fractions were concentrated in vacuo, sonicated in methanol and collected by filtration to afford yellow solid product. Next, it was recrystallized twice from acetonitrile (and a small amount of chloroform) to give the product as a crystalline yellow-orange solid (130.0 mg, 0.1816 mmol, 34%).

^{1}H NMR (400 MHz, $CDCl_3$) δ 8.21 (d, J = 30.3 Hz, 2H), 7.99 (s, 1H), 7.68 (d, J = 9.0 Hz, 1H), 7.62 (s, 2H), 7.51 (t, J = 8.2 Hz, 2H), 7.27 (s, 1H), 7.22 (d, J = 9.4 Hz, 2H), 6.88 (dd, J = 8.2, 2.2 Hz, 4H), 3.74 (t, J = 5.2 Hz, 8H), 1.09 – 0.96 (m, 8H), 0.57 – 0.41 (m, 4H), 0.36 – 0.26 (m, 8H). **HRMS** (ASAP-TOF): Calculated for $C_{44}H_{44}O_4{}^{81}Br^+$: 717.2423. Found m/z 717.2405 $[M+H]^+$.

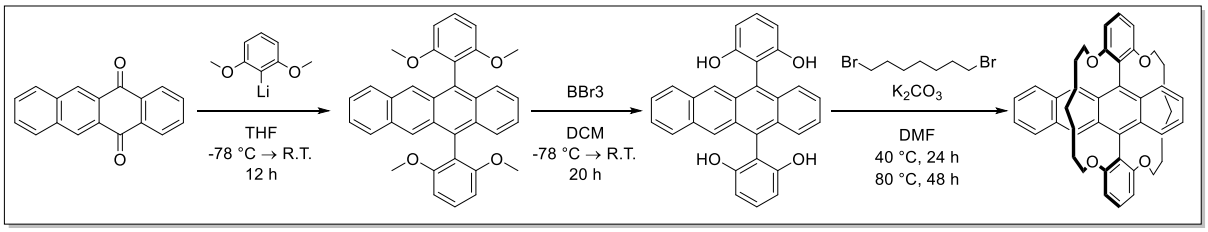

Scheme 2. Synthesis of Encapsulated Tetracene (**Encap-T**)

5,12-bis(2,6-dimethoxyphenyl)tetracene (Tet-OMe)

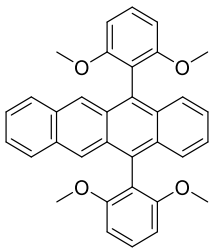

In a dry flask under argon at 0 ºC, n-BuLi (9.19 mL, 1.6 M, 14.7040 mmol) was added dropwise to a solution of 1,3-dimethoxybenzene (2.04 mL, 15.5776 mmol) and dry TMEDA (2.32 mL, 15.4733 mmol) in anhydrous THF (25 mL). Next, the reaction was warmed to room temperature and left stirring for 30 minutes. Next, the mixture was cooled to -78 ºC, after which solid 5,12-Naphthacenequinone (1.0 g, 3.8719 mmol) was added in one portion. The reaction was left to warm to room temperature and stirred for 12 h at room temperature. The reaction was quenched using saturated NH_4Cl solution and it was extracted with DCM (3 x). The combined organic layer was dried over $MgSO_4$, filtered and concentrated in vacuo. Next, the residue was re-dissolved in regular THF (~150 mL) and a solution of $SnCl_2$ x $2H_2O$ (4.2 g) in THF (180 mL) and glacial AcOH (30 mL). The reaction was left stirring for 3 h at room temperature. The resulting mixture was concentrated in vacuo (use toluene to co-evaporate AcOH). The residue was then dissolved in DCM (~200 mL) and washed with 1M HCl (2 x 100 mL). The aqueous layer was extracted with DCM (~100 mL) and the combined organic layer was dried over $MgSO_4$, filtered and concentrated in vacuo. The resulting residue was purified via silica column chromatography (stepwise column; starting with 100% hexane, then 15% DCM to remove leftover 1,3-dimethoxybenzene and finally 25 to 35% DCM to elute the product). The product fractions were concentrated in vacuo, after which the solids were sonicated in hexane (and a tiny amount of DCM) and collected by filtration to afford the product as a bright yellow solid (1.35 g, 2.6968 mmol, 70%).

^{1}H NMR (700 MHz, $CDCl_3$) δ 8.25 (s, 2H), 7.81 – 7.75 (m, 2H), 7.62 – 7.59 (m, 2H), 7.57 (t, J = 8.4 Hz, 2H), 7.22 (dd, J = 11.0, 8.6 Hz, 4H), 6.87 (d, J = 8.4 Hz, 4H), 3.57 (s, 6H). **HRMS** (ASAP-TOF): Calculated for $C_{34}H_{29}O_4^+$: 501.2066. Found m/z 501.2061 $[M+H]^+$.

Synthesis of 5,12-bis(resorcinol)tetracene (Tet-OH)

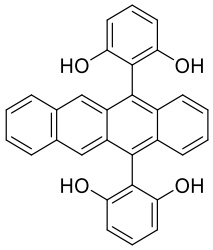

In a dry flask under argon at -78 ºC, BBr_3 (11.2 mL, 1.0 M, 11.2 mmol) was added dropwise to a solution of Tet-OMe (700 mg, 1.3983 mmol) in dry DCM (70 mL). The reaction was allowed to warm to room temperature and was stirred for 20 h (monitored by NMR). Next, the reaction mixture was poured into a stirring saturated $NaHCO_3$ solution (~200 mL) and the DCM layer was separated. Next, it was extracted with EtOAc (2 x 150 mL). The combined organic layers were concentrated in vacuo and purified via silica column chromatography (stepwise column; starting with 100% hexane, then going gradually to 100% DCM and finally 1, 2, 5 and 10% EtOAc). The product eluted with 5-10% EtOAc in DCM. The product fractions were concentrated in vacuo, after which the solids were sonicated in hexane (and a tiny amount of DCM) and collected by filtration to afford the product as an orange solid (358.6 mg, 0.8068 mmol, 58%).

^{1}H NMR (700 MHz, DMSO) δ 9.00 (s, 4H), 8.28 (s, 2H), 7.89 – 7.77 (m, 2H), 7.63 – 7.55 (m, 2H), 7.31 (d, J = 7.0 Hz, 2H), 7.26 (d, J = 7.2 Hz, 2H), 7.23 (t, J = 8.2 Hz, 2H), 6.64 (d, J = 8.2 Hz, 4H). **HRMS** (ASAP-TOF): Calculated for $C_{30}H_{21}O_4^+$: 445.1440. Found m/z 445.1432 $[M+H]^+$.

Synthesis of Encapsulated Tetracene (Encap-T)

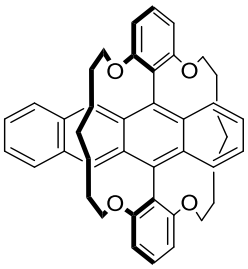

Under argon, 1,7-dibromoheptane (0.39 mL, 2.2826 mmol) was added to a mixture of Tet-OH (500 mg, 1.1249 mmol) and K_2CO_3 (777 mg, 5.6219 mmol) in dry DMF (220 mL) and the reaction mixture was heated to 40 ºC for 24 h and 80 ºC for 48 h. Next, it was concentrated in vacuo and the crude product was purified via silica column chromatography using 30-35% DCM in hexane. The product fractions were concentrated in vacuo, sonicated in methanol and collected by filtration to afford yellow solid product. Next, it was recrystallized from acetonitrile (and a small amount of chloroform) to give the product as a crystalline yellow-orange solid (287.6 mg, 0.4516 mmol, 40%).

^{1}H NMR (700 MHz, $CDCl_3$) δ 8.28 (s, 2H), 7.81 (dd, J = 6.5, 3.1 Hz, 2H), 7.61 (dd, J = 6.9, 3.2 Hz, 2H), 7.51 (t, J = 8.3 Hz, 2H), 7.22 (ddd, J = 24.8, 6.9, 2.9 Hz, 4H), 6.89 (d, J = 8.3 Hz, 4H), 3.74 (t, J = 5.3 Hz, 8H), 1.09 – 1.02 (m, 4H), 1.02 – 0.95 (m, 4H), 0.51 (dq, J = 13.8, 6.8 Hz, 2H), 0.43 (td, J = 13.7, 6.9 Hz, 2H), 0.37 – 0.30 (m, 4H), 0.30 – 0.25 (m, 4H). **HRMS** (ASAP-TOF): Calculated for $C_{44}H_{45}O_4^+$: 637.3318. Found m/z 637.3319 $[M+H]^+$. **mp:** 315–318 °C.

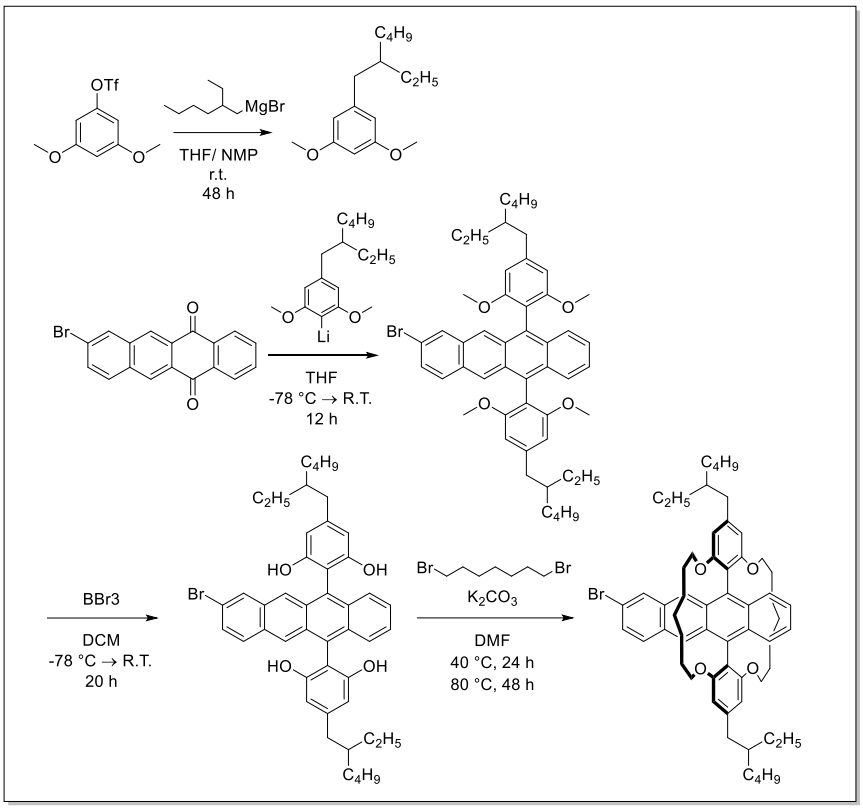

Scheme 3. Synthesis of Encapsulated Bromo Tetracene with alkyl group (E-EH-Br-Tet)

Synthesis of 3,5-Dimethoxyethylhexylbenzene.

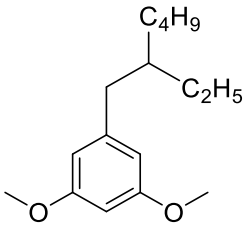

Ethylhexylmagnesium bromide (1.0 M in ether, 100 mL, 1.31 eq.) was added dropwise to a solution of 3,5-dimethoxyphenyl triflate (21.9 g, 76.5 mmol, 1.00 eq.) and $Fe(acac)_3$ (1.34 g, 3.79 mmol, 5 mol.%) in dry THF (450 mL) and dry NMP (43 mL) under argon at room temperature. The mixture was stirred overnight, and analysis by NMR indicated the starting material had not been completely consumed (note: residual triflate is very hard to remove by chromatography or distillation). Additional ethylhexylmagnesium bromide (20.0 mL, 0.26 eq.) and $Fe(acac)_3$ (1.34 g, 3.79 mmol, 5 mol.%) were added and the mixture stirred overnight. The reaction mixture was quenched with 1 M HCl (300 mL), diluted with hexane (200 mL) and the resulting mixture filtered through celite, eluting with further hexane (ca. 300 mL). The layers were separated and the aqueous layer further extracted with hexane (2 × 200 mL). The extracts were combined, dried over $MgSO_4$ and the solvent removed under reduced pressure. Notable impurities are 2-(ethyl)hexane and 1,3-dimethoxybenzene,, both of which are more volatile than the product. The residue was purified by distillation (0.5 mbar, 140 °C) to afford dimethoxyethylhexylbenzene (17.2 g, 68.9 mmol, 90%) as a colourless oil. Characterisation data were in agreement with the literature.[17]

^{1}H NMR (400 MHz, $CDCl_3$) δ 7.26 (s, 2H), 7.24 (s, 1H), 4.73 (s, 6H), 3.46 – 3.37 (m, 2H), 2.54 – 2.50 (m, 1H), 2.28 – 2.17 (m, 8H), 1.87 – 1.78 (m, 6H).

Synthesis of EH-Br-Tet-OMe

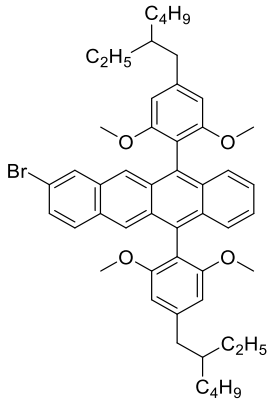

In a dry flask under argon at 0 ºC, n-BuLi (7.80 mL, 1.6 M, 12.48 mmol) was added dropwise to a solution of 1-(2-ethylhexyl)-3,5-dimethoxybenzene (3.30 g, 13.1799 mmol) and dry TMEDA (2.00 mL, 13.3391 mmol) in anhydrous THF (30 mL). Next, the reaction was warmed to room temperature and left stirring for 30 minutes. Next, the mixture was cooled to -78 ºC, after which solid 8-bromo-5,12-tetracenequinone (1.5 g, 4.4488 mmol) was added in one portion. The reaction was left to warm to room temperature and stirred for 12 h at room temperature. The reaction was quenched using saturated NH_4Cl solution and it was extracted with DCM (3 x). The combined organic layer was dried over $MgSO_4$, filtered and concentrated in vacuo. Next, a solution of $SnCl_2$ x $2H_2O$ (4.2 g) in THF (100 mL) and glacial AcOH (20 mL) was added to the residue. The reaction was left stirring for 3 h at room temperature. The resulting mixture was concentrated in vacuo (use toluene to co-evaporate AcOH). The residue was then dissolved in DCM (~200 mL) and washed with 1M HCl (2 x 100 mL). The aqueous layer was extracted with DCM (~100 mL) and the combined organic layer was dried over $MgSO_4$, filtered and concentrated in vacuo. The resulting residue was purified via silica column chromatography (stepwise column; starting with 100% hexane, then 10% DCM to remove leftover 1,3-dimethoxybenzene and finally 20-30% DCM to elute the product). The product fractions were concentrated in vacuo, after which the solids were sonicated in hexane (and a tiny amount of DCM) and collected by filtration to afford the product as a yellow solid (2.60 g, mmol, 73%).

^{1}H NMR (700 MHz, CD_2Cl_2) δ 8.24 (d, J = 53.3 Hz, 2H), 8.01 (s, 1H), 7.72 (d, J = 9.1 Hz, 1H), 7.64 (s, 2H), 7.34 (d, J = 9.1 Hz, 1H), 7.28 (d, J = 9.5 Hz, 2H), 6.77 (s, 4H), 3.67 (s, 12H), 2.82 (qd, J = 13.0, 7.5 Hz, 4H), 1.88 (s, 2H), 1.61 – 1.54 (m, 6H), 1.47 (dd, J = 27.6, 22.5 Hz, 12H), 1.08 (td, J = 7.4, 3.8 Hz, 6H), 1.02 (q, J = 6.6 Hz, 6H). **HRMS** (ASAP-TOF): Calculated for $C_{50}H_{59}BrO_4^+$: 802.3597. Found m/z 802.3560 $[M]^+$.

Synthesis of EH-Br-Tet-OH

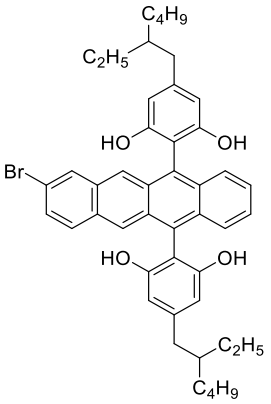

In a dry flask under argon at -78 ºC, BBr_3 (12.0 mL, 1.0 M, 12.0 mmol) was added dropwise to a solution of EH-Br-Tet-OMe (1.10 g, 1.3683 mmol) in dry DCM (100 mL). The reaction was allowed to warm to room temperature and was stirred for 20 h (monitored by NMR). Next, the reaction mixture was poured into a stirring saturated $NaHCO_3$ solution (~200 mL) and the DCM layer was separated. Next, it was extracted with DCM (2 x 150 mL). The combined organic layers were concentrated in vacuo and purified via silica column chromatography using 60-70% DCM in hexane. The product fractions were concentrated in vacuo, after which the solids were sonicated in hexane (and a tiny amount of DCM) and collected by filtration to afford the product as a yellow-orange solid (719.5 mg, 0.9621 mmol, 70%).

^{1}H NMR (700 MHz, DMSO) δ 8.94 (d, J = 7.7 Hz, 4H), 8.28 (d, J = 27.6 Hz, 2H), 8.14 (s, 1H), 7.82 (d, J = 9.1 Hz, 1H), 7.63 – 7.59 (m, 2H), 7.37 (d, J = 9.0 Hz, 1H), 7.28 (d, J = 9.8 Hz, 2H), 6.46 (s, 4H), 2.54 (dd, J = 12.7, 6.3 Hz, 4H), 1.69 (s, 2H), 1.45 – 1.34 (m, 16H), 0.99 – 0.93 (m, 12H). **HRMS** (ASAP-TOF): Calculated for $C_{46}H_{52}BrO_4^+$: 747.3049. Found m/z 747.3029 $[M+H]^+$.

Synthesis of E-EH-Br-Tet

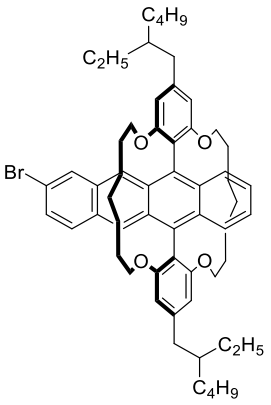

Under argon, 1,7-dibromoheptane (0.325 mL, 1.9022 mmol) was added to a mixture of EH-Br-Tet-OH (670 mg, 0.8959 mmol) and K_2CO_3 (622 mg, 4.5004 mmol) in dry DMF (180 mL) and the reaction mixture was heated to 40 ºC for 24 h and 80 ºC for 48 h. Next, it was concentrated in vacuo, re-dissolved in DCM and washed with water and brine (2 x). The organic layer was dried over $MgSO_4$ and concentrated in vacuo. The crude product was purified via silica column chromatography using 20% DCM in hexane. The product fractions were concentrated in vacuo, sonicated in methanol and collected by filtration to afford yellow solid product (427 mg, 0.4542 mmol, 51%).

^{1}H NMR (400 MHz, CD2Cl2) δ 8.27 (d, J = 32.0 Hz, 2H), 8.02 (s, 1H), 7.73 (d, J = 9.2 Hz, 1H), 7.66 (dd, J = 8.5, 6.3 Hz, 2H), 7.32 (dd, J = 9.1, 1.7 Hz, 1H), 7.27 (dd, J = 6.9, 3.2 Hz, 2H), 6.75 (s, 4H), 3.82 – 3.74 (m, 8H), 2.76 (p, J = 6.0 Hz, 4H), 1.82 (d, J = 5.7 Hz, 2H), 1.47 – 1.41 (m, 6H), 1.05 (td, J = 7.4, 2.2 Hz, 8H), 0.51 (ddt, J = 20.1, 13.2, 6.6 Hz, 4H), 0.36 – 0.27 (m, 8H). **HRMS** (ASAP-TOF): Calculated for $C_{60}H_{76}BrO_4^+$: 939.4927. Found m/z 939.4922 $[M+H]^+$.

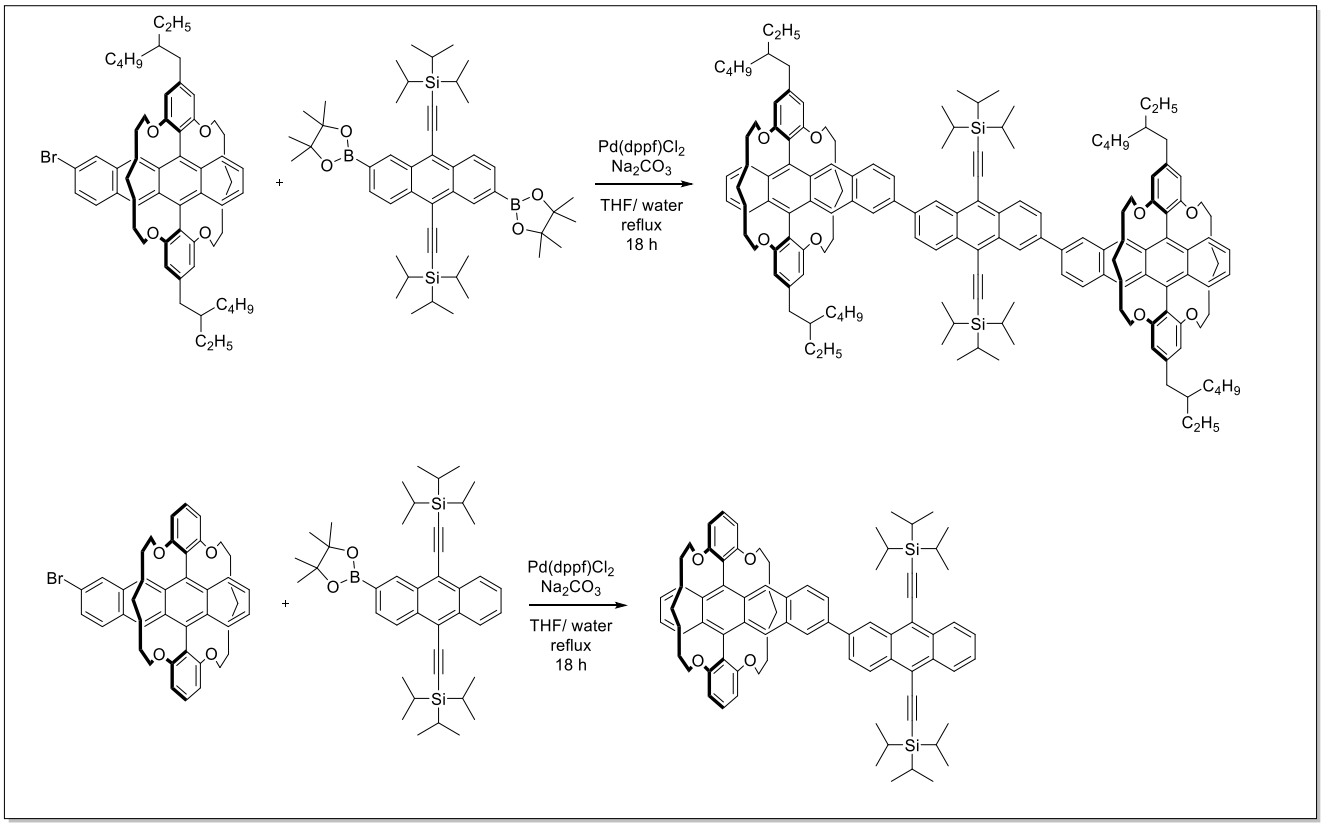

Scheme 3. Synthesis of **Encap-TAT** and **Encap-TA**

Synthesis of Encap-TA

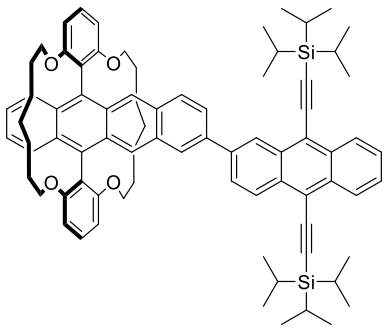

A mixture of E-Tet-Br (50 mg, 0.07 mmol, 1.00 eq.), BPin-TIPS-anthracene (51.1 mg, 0.08 mmol, 1.10 eq.)) and $Pd(dppf)Cl_2$ (5 mol.%) and 2 M Na_2CO_3 (0.5 mL) in THF (10 mL) was heated to reflux under argon overnight. The mixture was cooled to room temperature, diluted with sat. NH_4Cl (50 mL) and extracted with DCM (3 × 20 mL). The extracts were combined, dried over $MgSO_4$ and the solvent evaporated under reduced pressure. The residue was purified by flash chromatography using 0-100% DCM in hexane. The product fractions were concentrated in vacuo, and then recrystallised twice from DCM in ethanol to afford the product as an orange solid (12.3 mg, 5 µmol, 15%).

^{1}H NMR (500 MHz, $CDCl_3$) δ 9.09 (d, J = 1.4 Hz, 1H), 8.72 (d, J = 9.0 Hz, 1H), 8.67 – 8.63 (m, J = 7.2, 5.6, 3.6 Hz, 2H), 8.42 (s, 1H), 8.34 (s, 2H), 8.12 (dd, J = 9.0, 1.8 Hz, 1H), 7.99 (d, J = 9.0 Hz, 1H), 7.87 – 7.83 (m, 1H), 7.68 – 7.64 (m, J = 8.7, 6.1, 2.8 Hz, 2H), 7.63 – 7.60 (m, 2H), 7.57 – 7.53 (m, J = 8.0, 4.0 Hz, 2H), 7.27 – 7.22 (m, J = 6.2, 3.0 Hz, 2H), 6.93 (t, J = 8.0 Hz, 4H), 3.82 – 3.77 (m, 8H), 1.15 – 1.04 (m, 8H), 0.60 – 0.46 (m, 4H), 0.43 – 0.31 (m, 8H). **HRMS** (ASAP-TOF): Calculated for $C_{80}H_{93}O_4Si_2^+$1173.6612. Found m/z 1173.6591 $[M+H]^+$.
^{13}C NMR spectra were not obtained due to the limited solubility of the material. **mp:** 210–213 °C.

Synthesis of Encap-TAT

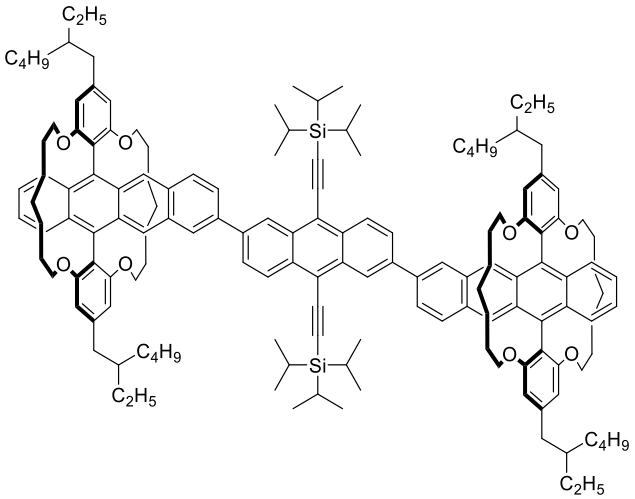

A mixture of E-EH-Br-Tet (100 mg, 0.11 mmol, 2.20 eq.), bis(BPin)-TIPS-anthracene (38.3 mg, 0.05 mmol, 1.00 eq.)) and $Pd(dppf)Cl_2$ (5 mol.%) and 2 M Na_2CO_3 (0.5 mL) in THF (10 mL) was heated to reflux under argon overnight. The mixture was cooled to room temperature, diluted with sat. NH_4Cl (50 mL) and extracted with DCM (3 × 20 mL). The extracts were combined, dried over $MgSO_4$ and the solvent evaporated under reduced pressure. The residue was purified by flash chromatography using 0-100% DCM in hexane and then by preparative HPLC using DCM in hexane on Phenomenex ic-5 column. The product fractions were concentrated in vacuo, and then recrystallised twice from DCM in methanol to afford the product as an orange solid (11.6 mg, 5 µmol, 10%).

^{1}H NMR (500 MHz, C_6D_6) δ 9.25 (d, J = 1.8 Hz, 2H), 8.92 (s, 2H), 8.87 (d, J = 9.0 Hz, 2H), 8.84 (s, 2H), 8.14 (s, 2H), 8.07 – 8.03 (m, 4H), 7.72 – 7.67 (m, 4H), 7.58 (dd, J = 9.0, 1.8 Hz, 2H), 7.10 – 7.07 (m, 4H), 6.96 (s, 4H), 6.92 (s, 4H), 3.82 – 3.78 (m, 4H), 3.76 – 3.70 (m, 12H), 2.90 (dd, J = 15.4, 7.1 Hz, 8H), 1.97 (dd, J = 12.0, 6.0 Hz, 4H), 1.46 – 1.42 (m, 18H), 1.39 (d, J = 5.4 Hz, 36H), 1.08 (d, J = 7.4 Hz, 12H), 1.03 – 1.01 (m, 12H),0.38 (s, 6H). **HRMS** (ASAP-TOF): Calculated for $C_{156}H_{199}O_8Si_2^+$ 2256.4698. Found m/z 2256.4734 $[M+H]^+$. **mp:** >350 °C (decomp.).
^{13}C NMR spectra were not obtained due to the limited solubility of the material.

NMR Spectroscopy

8-bromo-5,12-tetracenequinone

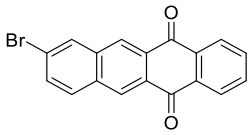

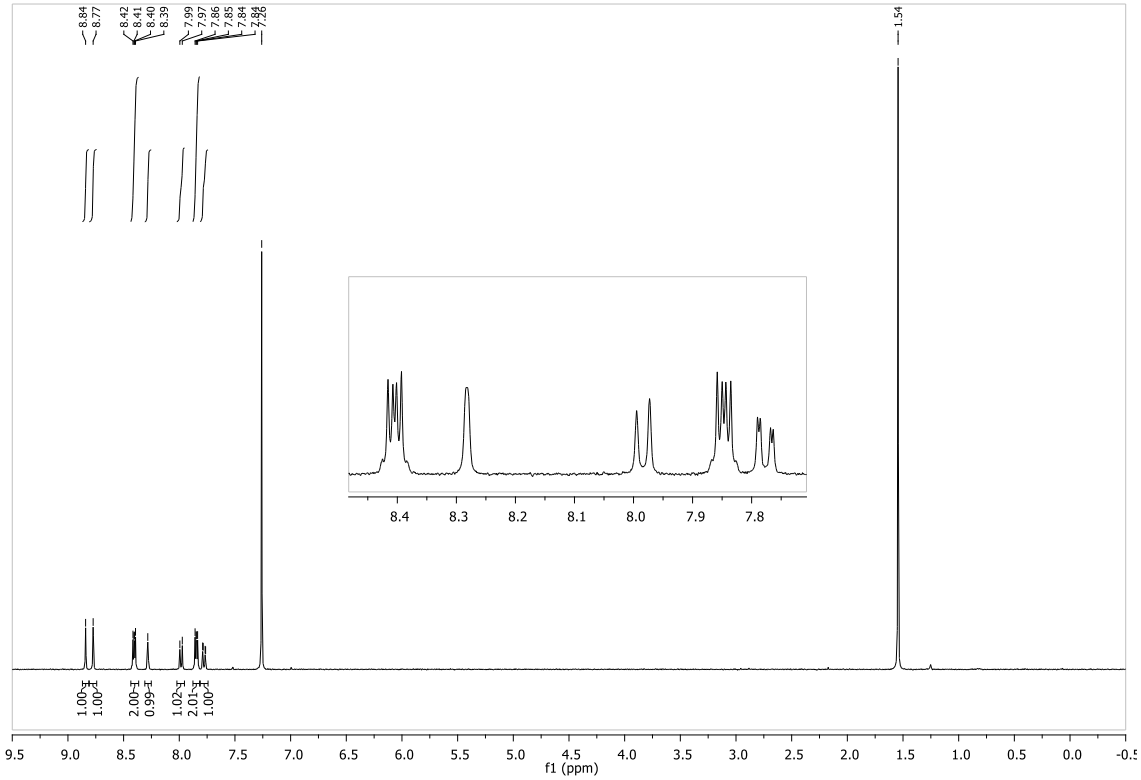

8-bromo-5,12-bis(2,6-dimethoxyphenyl)tetracene (Br-Tet-OMe)

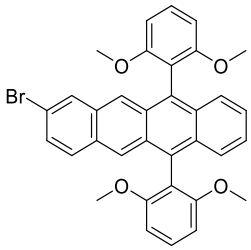

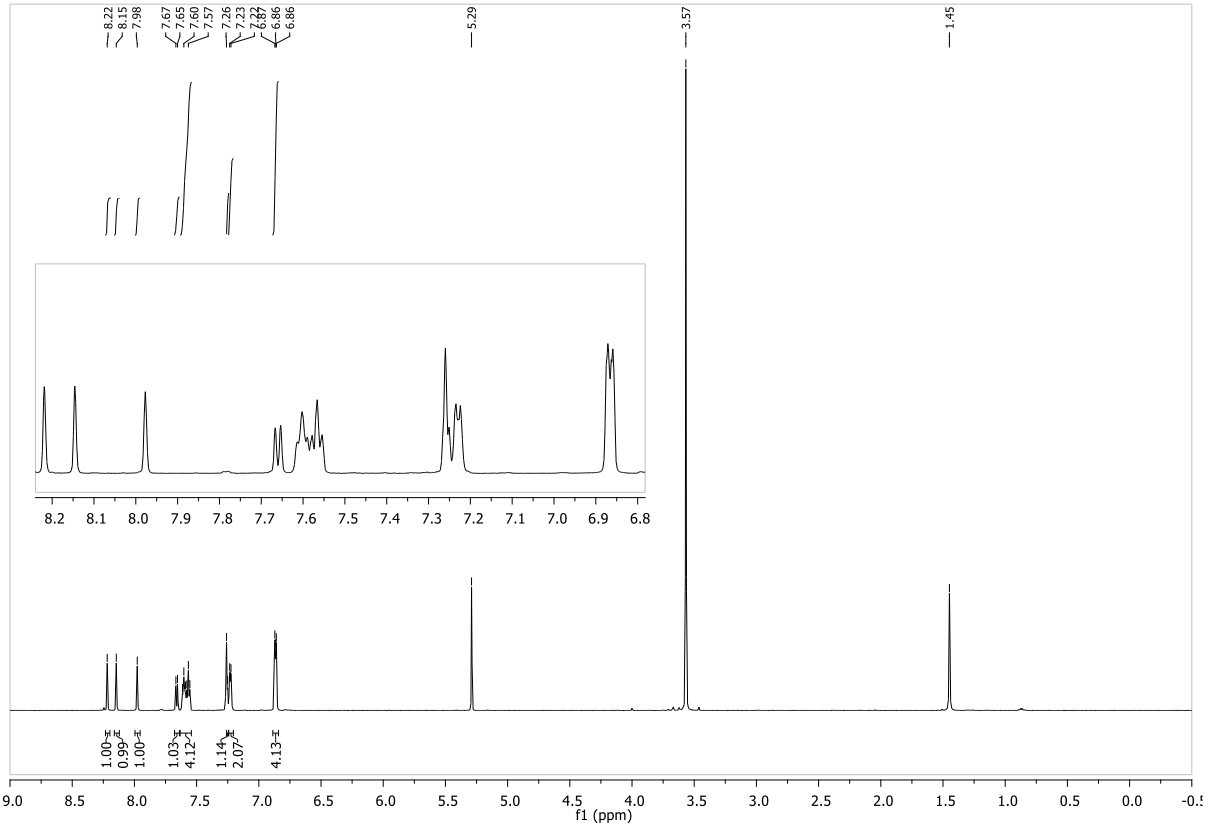

8-bromo-5,12-bis(resorcinol)tetracene (Br-Tet-OH)

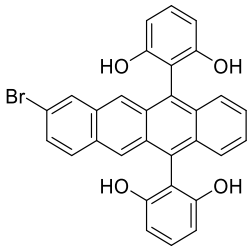

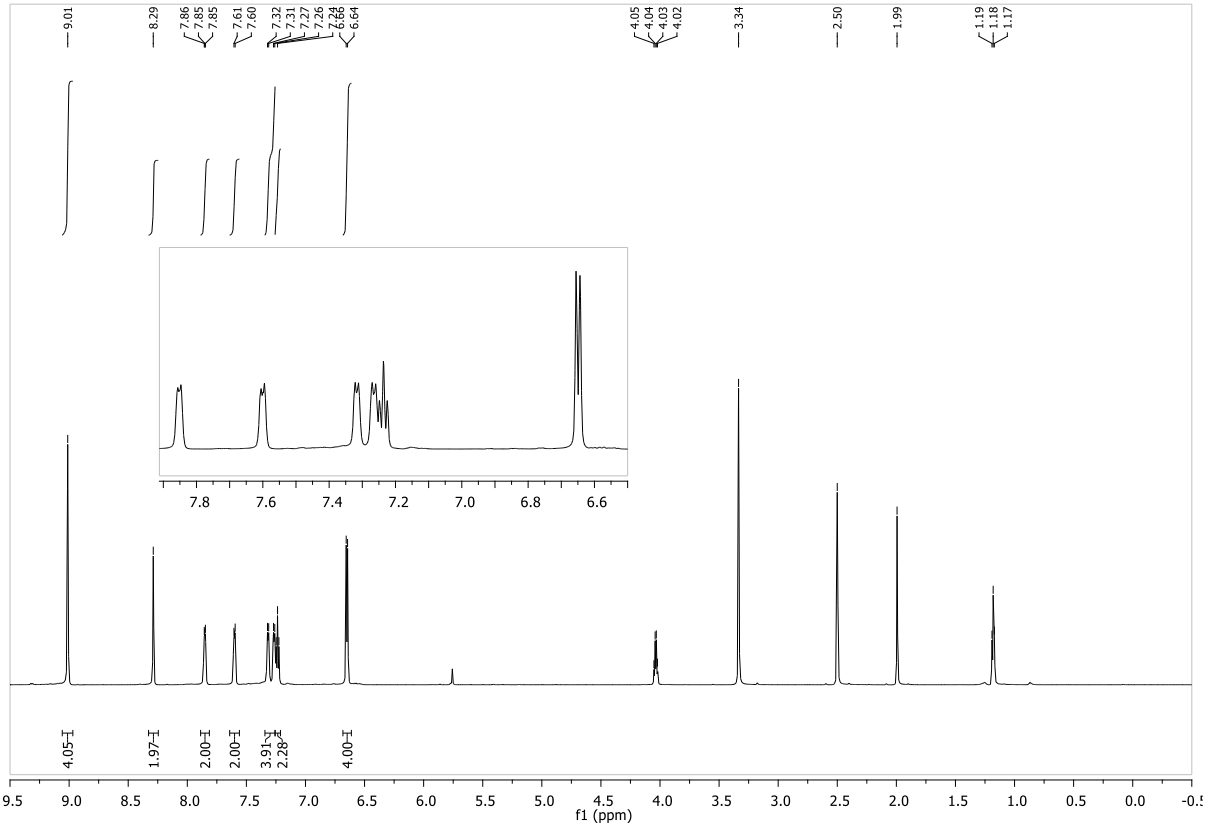

Encapsulated Bromo Tetracene (E-Tet-Br)

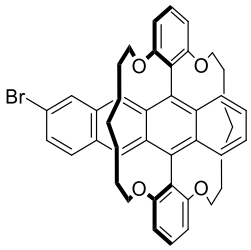

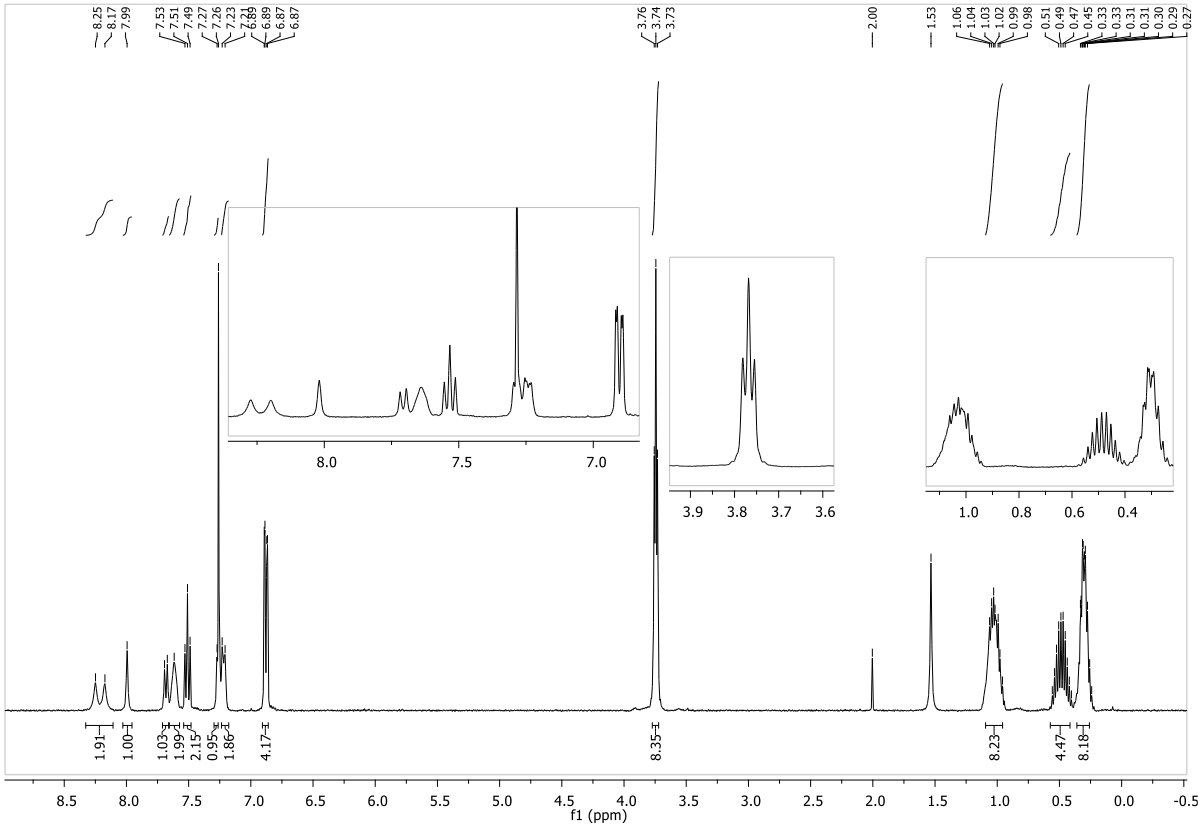

5,12-bis(2,6-dimethoxyphenyl)tetracene (Tet-OMe)

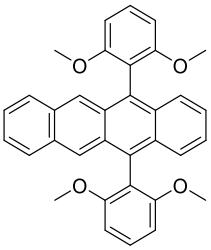

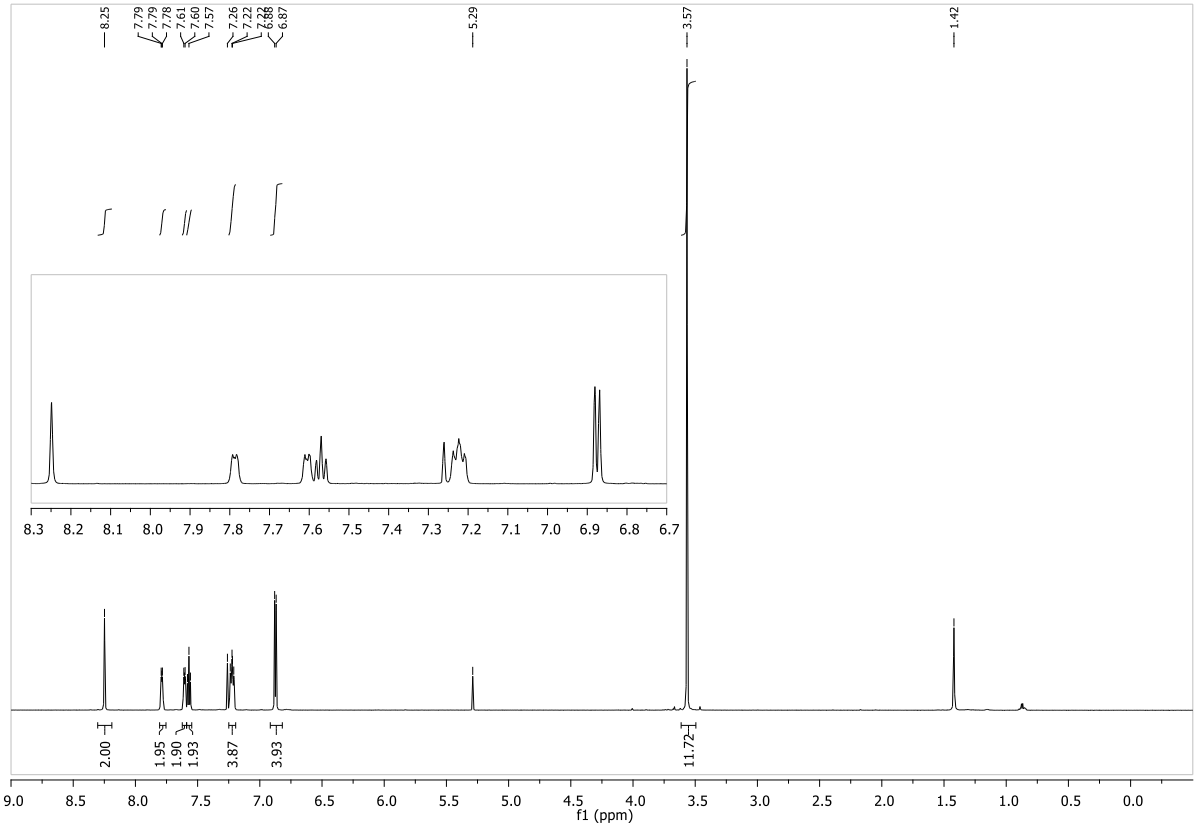

5,12-bis(resorcinol)tetracene (Tet-OH)

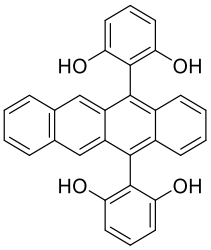

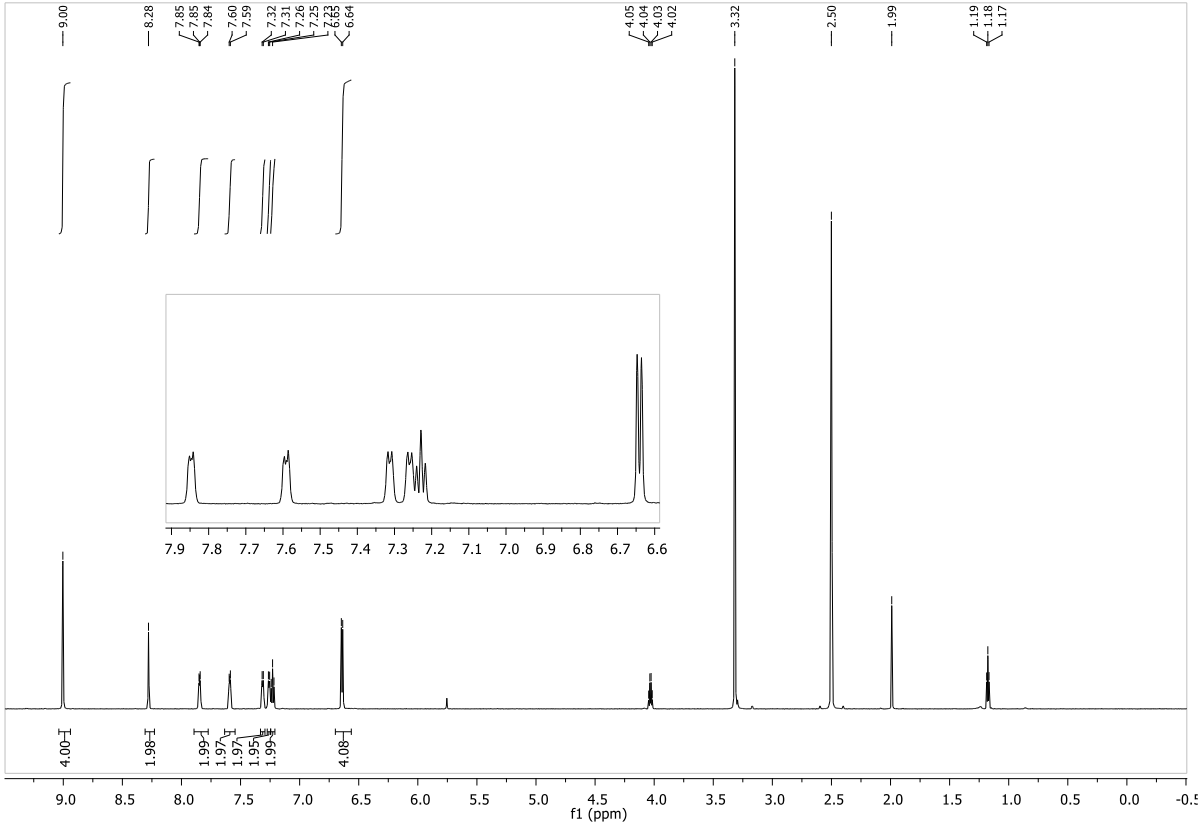

Encapsulated Tetracene (E-Tet)

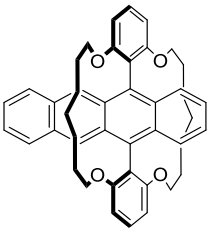

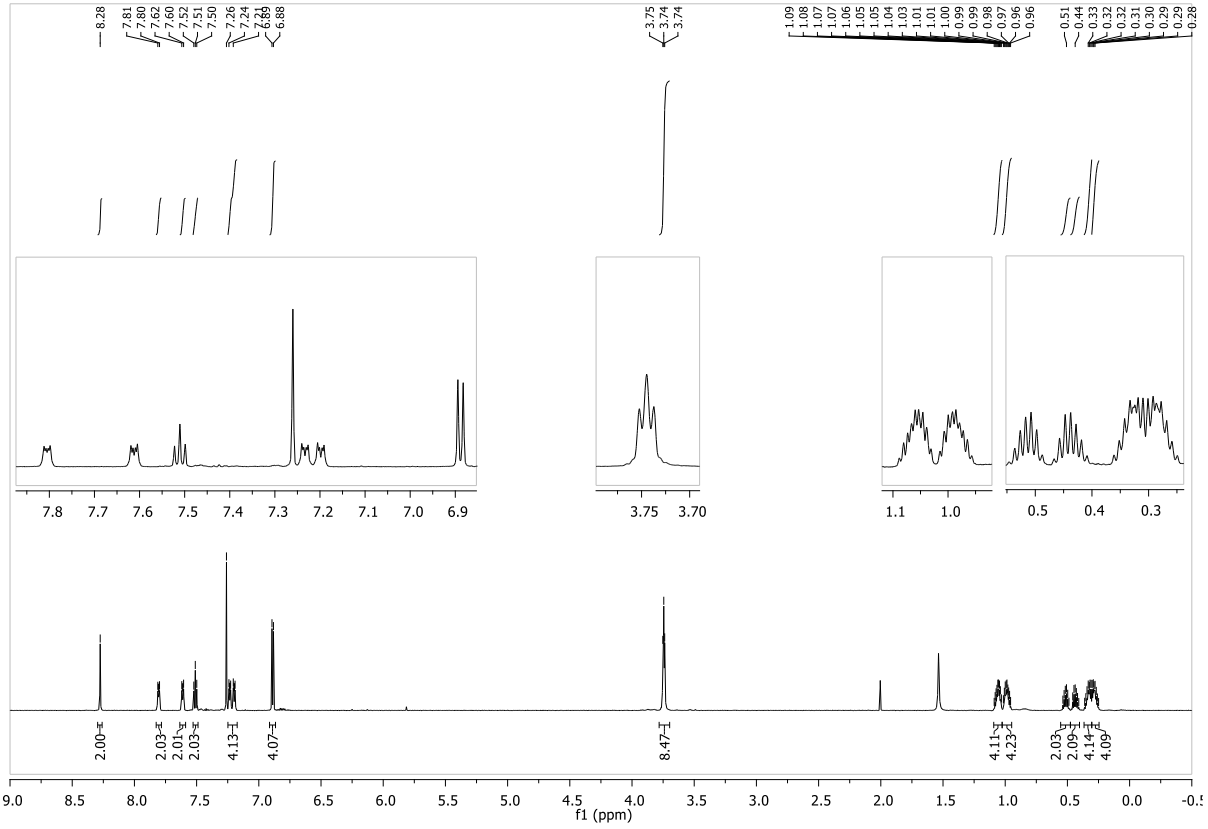

3,5-Dimethoxyethylhexylbenzene

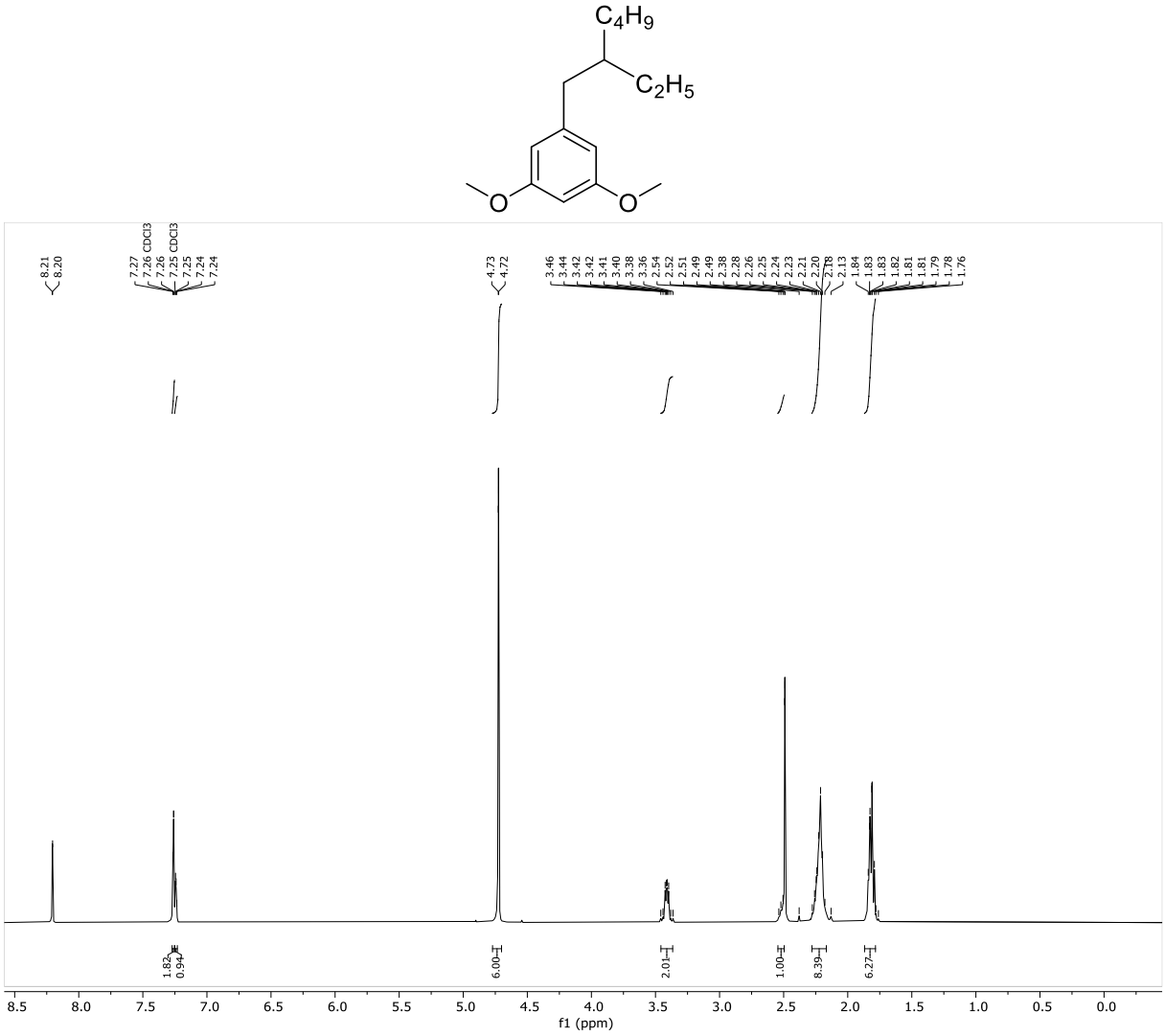

EH-Br-Tet-OMe

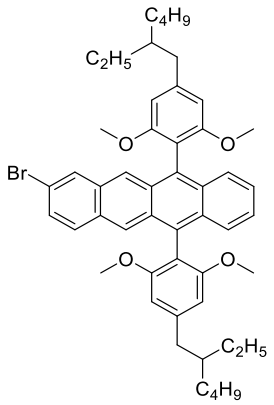
C4H9
C2H5
O
O
Br
O
O
C2H5
C4H9

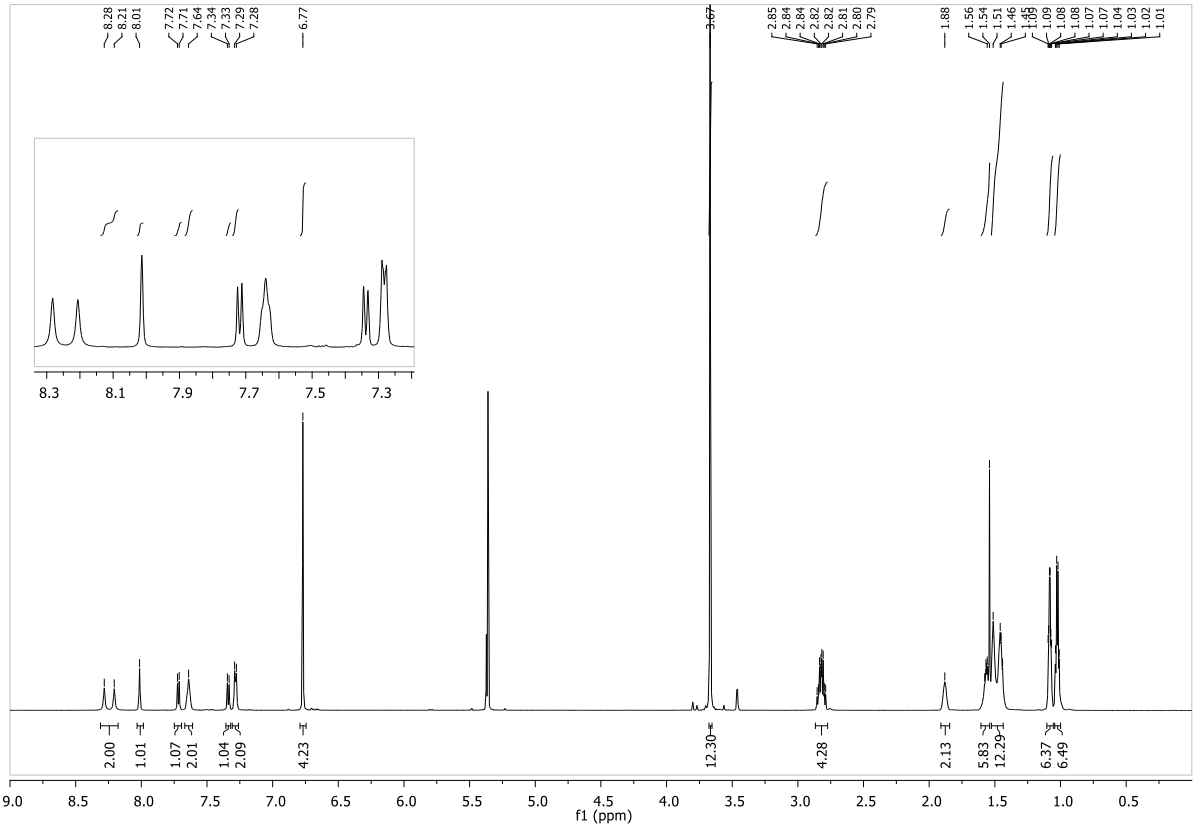
8.28
8.21
8.01
7.72
7.71
7.64
7.34
7.33
7.29
7.28
6.77
3.67
2.85
2.84
2.84
2.82
2.82
2.81
2.80
2.79
1.88
1.56
1.54
1.51
1.46
1.09
1.08
1.08
1.07
1.07
1.04
1.03
1.02
1.01
8.3
8.1
7.9
7.7
7.5
7.3
2.00
1.01
1.07
2.01
1.04
2.09
4.23
12.30
4.28
2.13
5.83
12.29
6.37
6.49
9.0
8.5
8.0
7.5
7.0
6.5
6.0
5.5
5.0
4.5
4.0
3.5
3.0
2.5
2.0
1.5
1.0
0.5
f1 (ppm)

EH-Br-Tet-OH

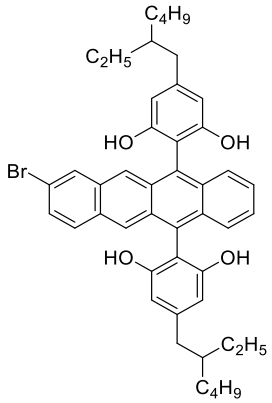
C4H9
C2H5
HO
OH
Br
HO
OH
C2H5
C4H9

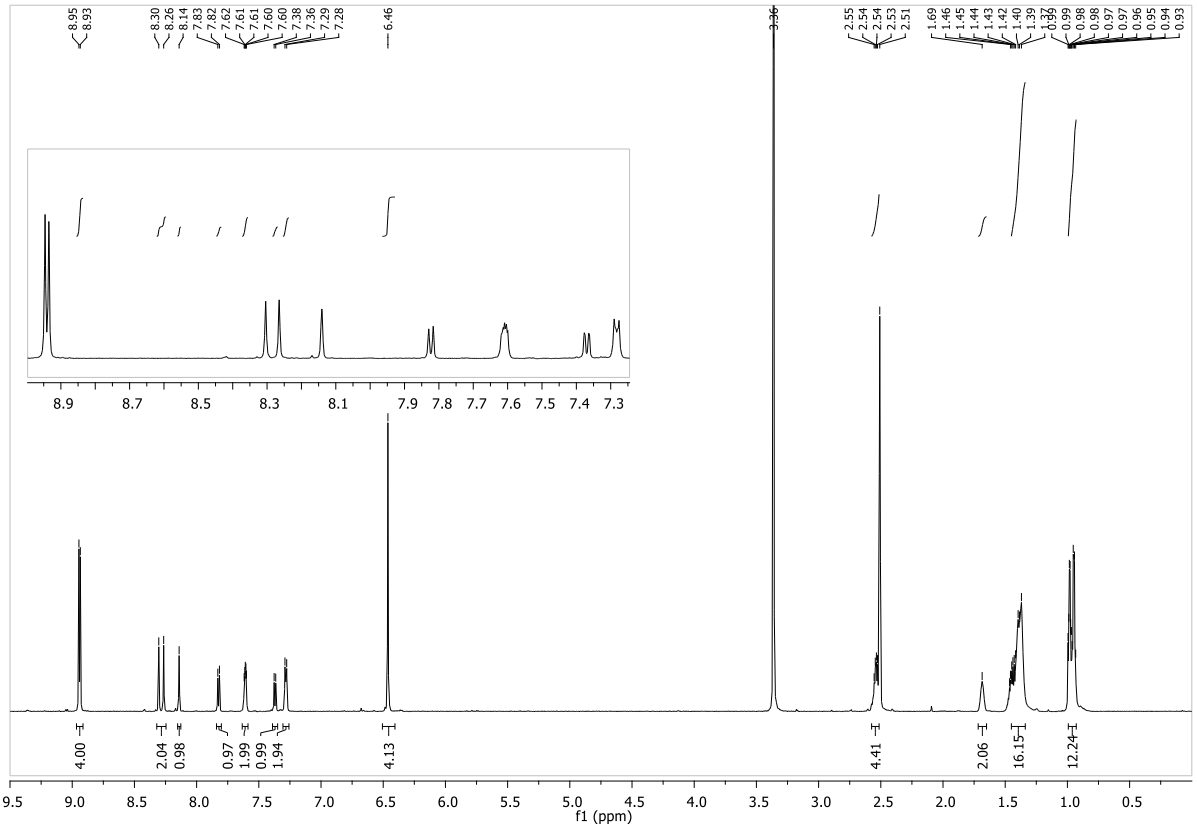
8.95
8.93
8.30
8.26
8.14
7.83
7.82
7.62
7.61
7.61
7.60
7.60
7.38
7.36
7.29
7.28
6.46
3.36
2.55
2.54
2.54
2.53
2.51
1.69
1.46
1.45
1.44
1.43
1.42
1.40
1.39
0.99
0.98
0.98
0.97
0.97
0.96
0.95
0.94
0.93
4.00
2.04
0.98
0.97
1.99
0.99
1.94
4.13
4.41
2.06
16.15
12.24
f1 (ppm)

E-EH-Br-Tet

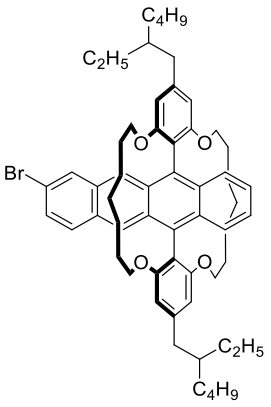
C4H9
C2H5
Br
O
O
O
O
C2H5
C4H9

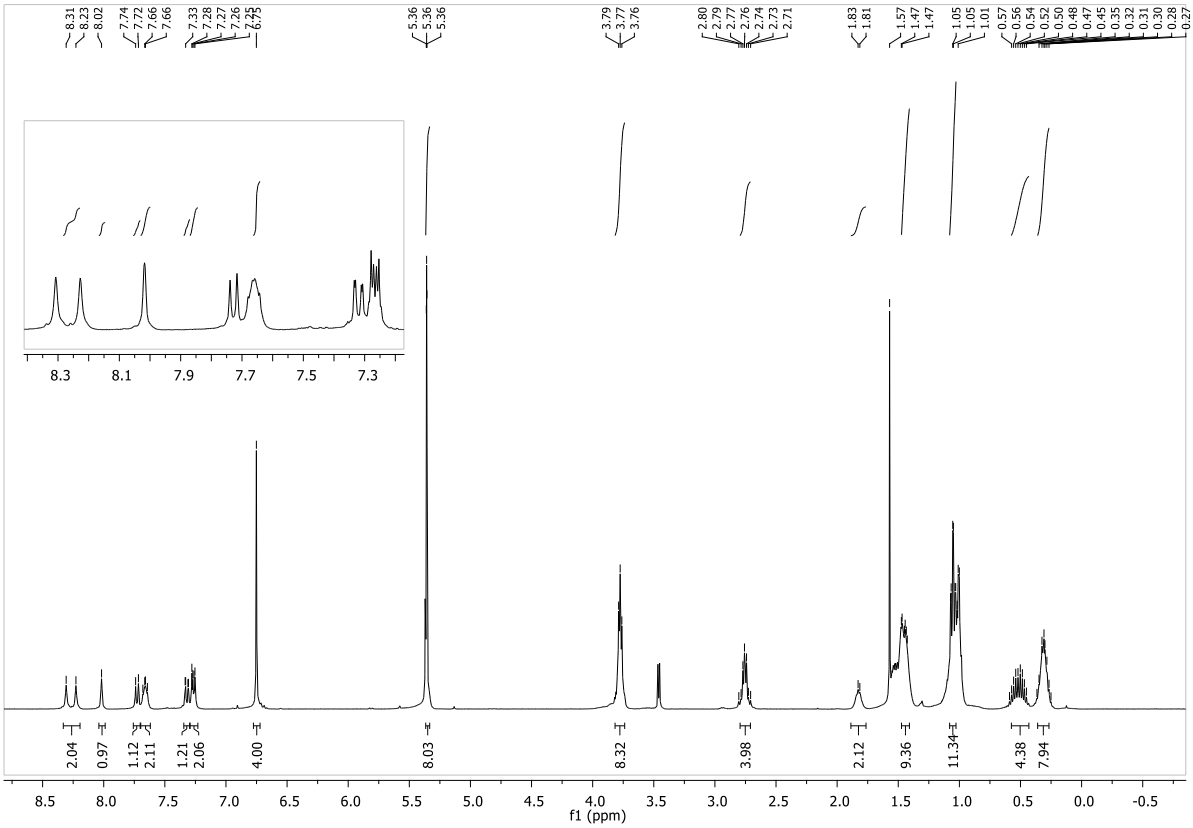
8.31
8.23
8.02
7.74
7.72
7.66
7.66
7.33
7.28
7.27
7.26
6.75
5.36
5.36
5.36
3.79
3.77
3.76
2.80
2.79
2.77
2.76
2.74
2.73
2.71
1.83
1.81
1.57
1.47
1.47
1.05
1.05
1.01
0.57
0.56
0.54
0.52
0.50
0.48
0.47
0.45
0.35
0.32
0.31
0.30
0.28
0.27
8.3
8.1
7.9
7.7
7.5
7.3
2.04
0.97
1.12
2.11
1.21
2.06
4.00
8.03
8.32
3.98
2.12
9.36
11.34
4.38
7.94
8.5
8.0
7.5
7.0
6.5
6.0
5.5
5.0
4.5
4.0
3.5
3.0
2.5
2.0
1.5
1.0
0.5
0.0
-0.5
f1 (ppm)

Encap-TA

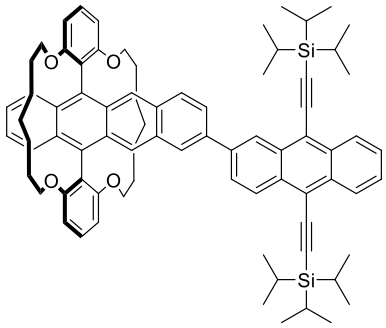
O
O
O
O
Si
Si

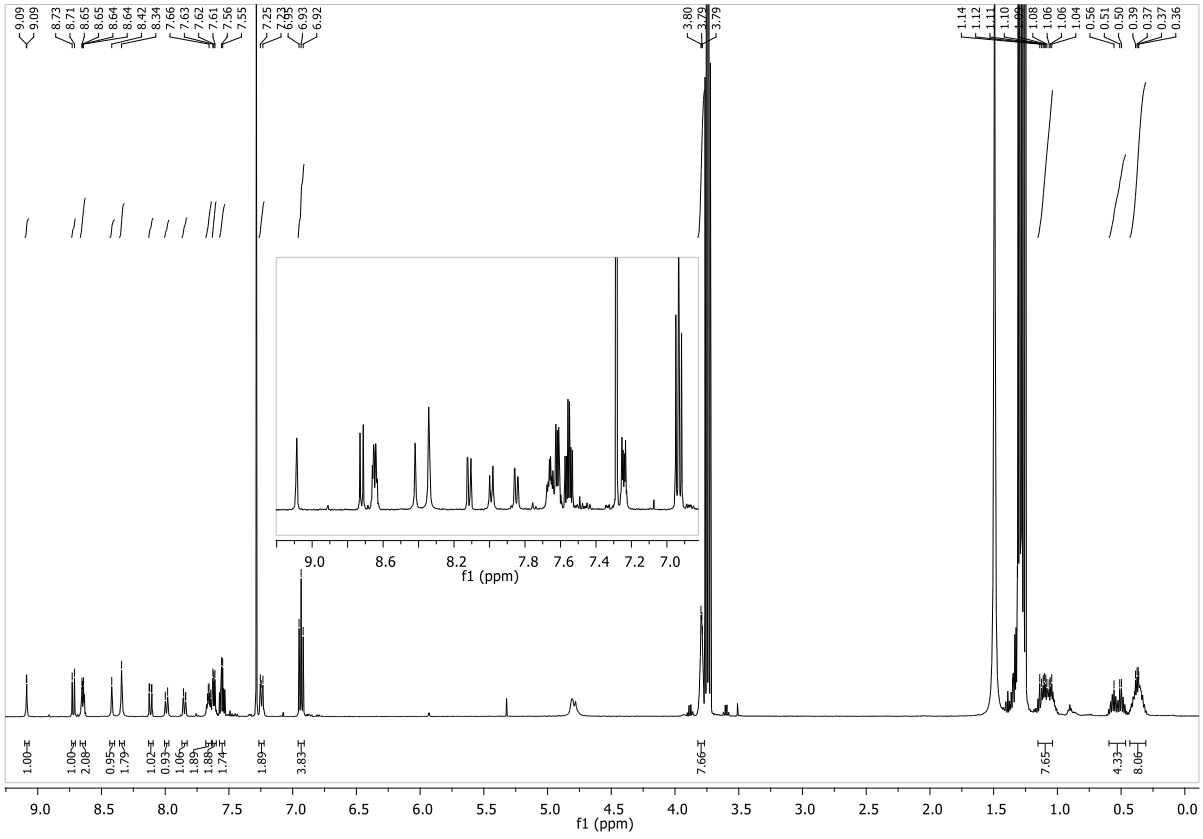
9.09
9.09
8.73
8.71
8.65
8.65
8.64
8.64
8.42
8.34
7.66
7.63
7.62
7.61
7.56
7.55
7.25
6.93
6.92
3.80
3.79
3.79
1.14
1.12
1.11
1.10
1.08
1.06
1.06
1.04
0.56
0.51
0.50
0.39
0.37
0.37
0.36
9.0
8.6
8.2
7.8
7.6
7.4
7.2
7.0
f1 (ppm)
1.00
1.00
2.08
0.95
1.79
1.02
0.93
1.06
1.89
1.84
1.74
1.89
3.83
7.66
7.65
4.33
8.06
9.0
8.5
8.0
7.5
7.0
6.5
6.0
5.5
5.0
4.5
4.0
3.5
3.0
2.5
2.0
1.5
1.0
0.5
0.0
f1 (ppm)

Single Mass Analysis
Tolerance = 200.0 PPM / DBE: min = -1.5, max = 50.0
Element prediction: Off
Number of isotope peaks used for i-FIT = 3

Monoisotopic Mass, Even Electron Ions
5 formula(e) evaluated with 1 results within limits (up to 50 closest results for each mass)
Elements Used:
C: 0-80 H: 0-93 O: 0-4 Si: 0-2

HAB_52700 SM4-72 S MONTANARO 2189 (4.699) Cm (2151:2326)

1: TOF MS ASAP+
1.36e+004

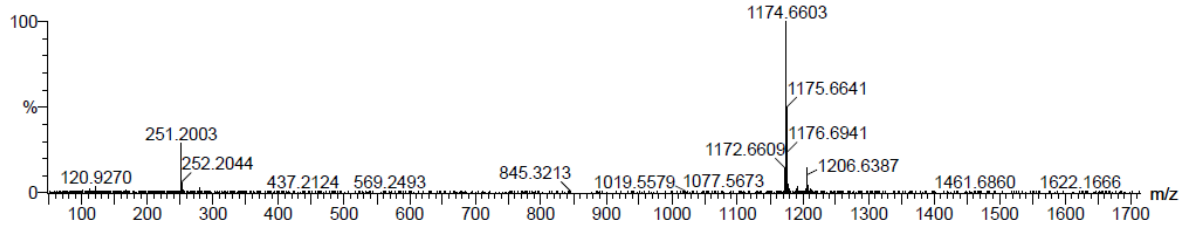

Minimum:				-1.5				
Maximum:		5.0	200.0	50.0				
Mass	Calc. Mass	mDa	PPM	DBE	i-FIT	Norm	Conf(%)	Formula
1173.6591	1173.6612	-2.1	-1.8	36.5	120.4	n/a	n/a	C80 H93 O4 Si2

Encap-TAT

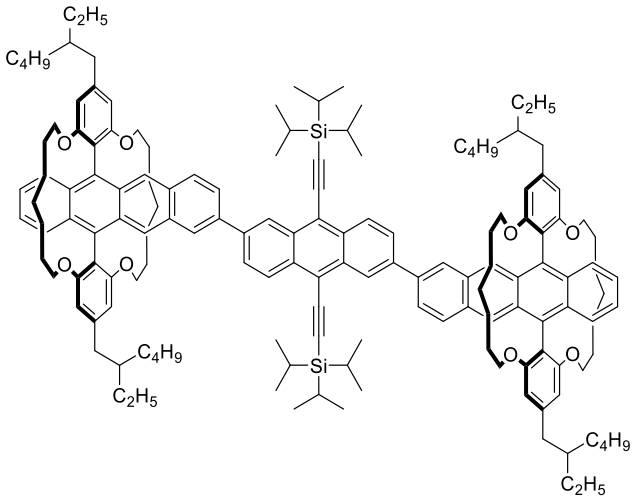
C2H5
C4H9
Si
O

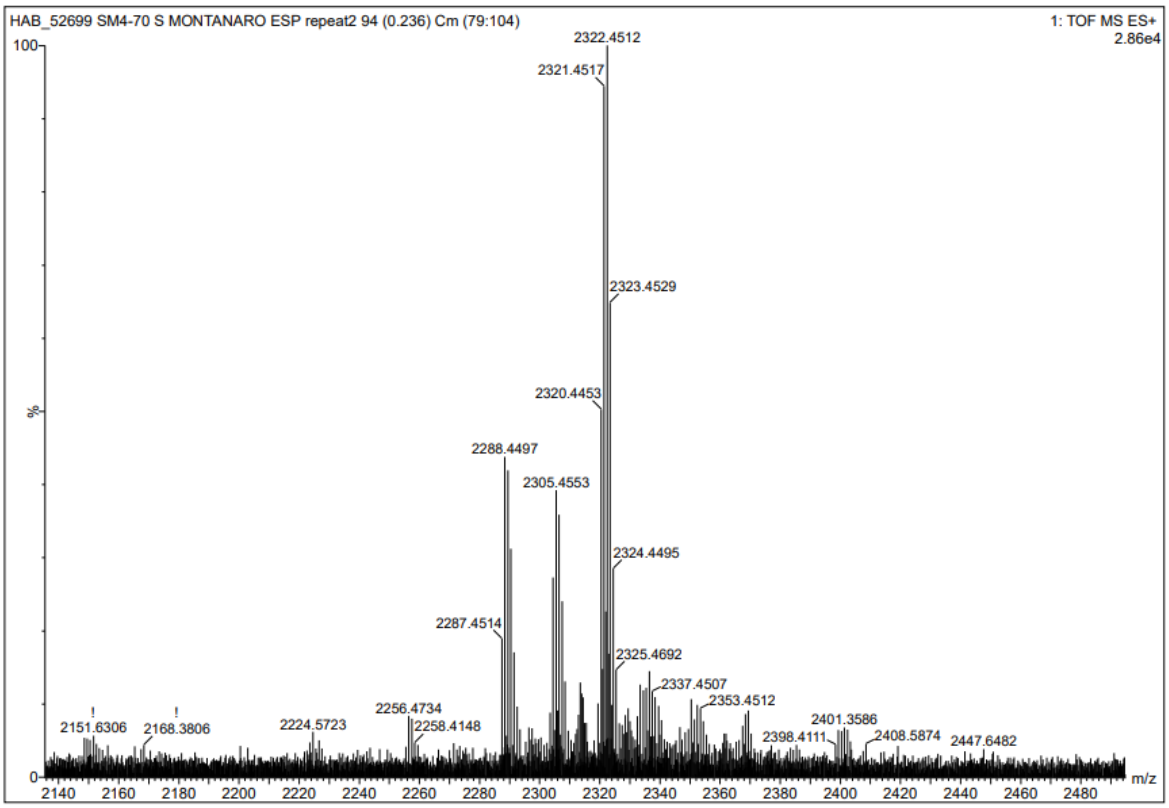
HAB_52699 SM4-70 S MONTANARO ESP repeat2 94 (0.236) Cm (79:104)
1: TOF MS ES+
2.86e4
100
%
0
2322.4512
2321.4517
2323.4529
2320.4453
2288.4497
2305.4553
2324.4495
2287.4514
2325.4692
2337.4507
2353.4512
2401.3586
2398.4111
2408.5874
2447.6482
2151.6306
2168.3806
2224.5723
2256.4734
2258.4148
m/z
2140 2160 2180 2200 2220 2240 2260 2280 2300 2320 2340 2360 2380 2400 2420 2440 2460 2480

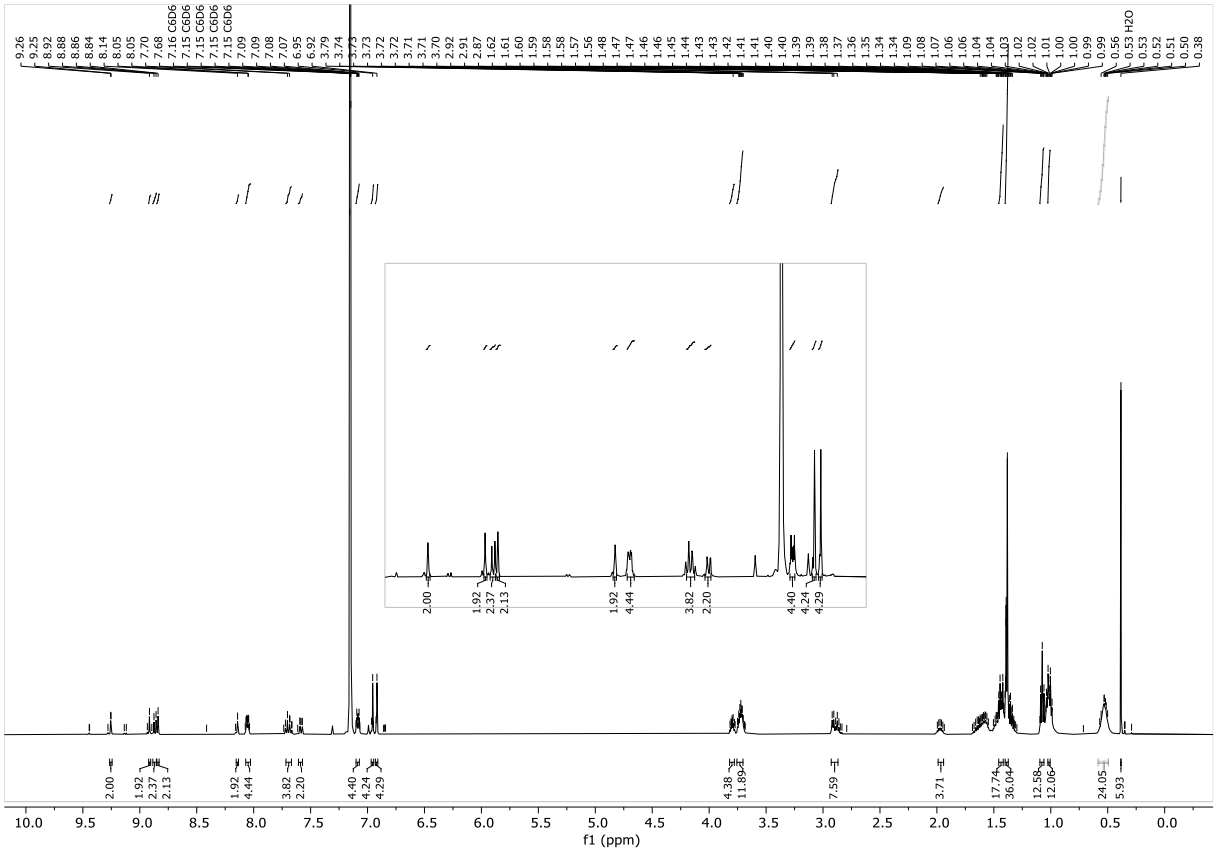
f1 (ppm)

Reference

(1) Citation | Gaussian.com. https://gaussian.com/citation/ (accessed 2025-08-01).

(2) Eich, ll M.; Beisinghoff, H.; Knodler Ohl, R. M.; Sprave, M.; Vydra, J.; Eckl, M.; Dorr, M.; Zentel, R.; Ahlheim, M.; Stahelin, M.; Zysset Lidng R Levenson J Zyss, B. J.; John de Mello, B. C.; Felix Wittmann, H. An Improved Experimental Determination of External Photoluminescence Quantum Efficiency. Advanced Materials **1997**, 9 (3), 230–232. https://doi.org/10.1002/ADMA.19970090308.

(3) Van Stokkum, I. H. M.; Larsen, D. S.; Van Grondelle, R. Global and Target Analysis of Time-Resolved Spectra. Biochimica et Biophysica Acta (BBA) - Bioenergetics **2004**, 1657 (2–3), 82–104. https://doi.org/10.1016/J.BBABIO.2004.04.011.

(4) Snellenburg, J. J.; Laptenok, S.; Seger, R.; Mullen, K. M.; van Stokkum, I. H. M. Glotaran: A Java-Based Graphical User Interface for the R Package TIMP. J Stat Softw **2012**, 49, 1–22. https://doi.org/10.18637/JSS.V049.I03.

(5) Kaufmann, C.; Bialas, D.; Stolte, M.; Würthner, F. Discrete Ï€-Stacks of Perylene Bisimide Dyes within Folda-Dimers: Insight into Long- and Short-Range Exciton Coupling. J Am Chem Soc **2018**, 140 (31), 9986–9995. https://doi.org/10.1021/JACS.8B05490/ASSET/IMAGES/LARGE/JA-2018-05490E_0005.JPEG.

(6) Weigend, F.; Ahlrichs, R. Balanced Basis Sets of Split Valence, Triple Zeta Valence and Quadruple Zeta Valence Quality for H to Rn: Design and Assessment of Accuracy. Physical Chemistry Chemical Physics **2005**, 7 (18), 3297–3305. https://doi.org/10.1039/B508541A.

(7) Chai, J. Da; Head-Gordon, M. Long-Range Corrected Hybrid Density Functionals with Damped Atom–Atom Dispersion Corrections. Physical Chemistry Chemical Physics **2008**, 10 (44), 6615–6620. https://doi.org/10.1039/B810189B.

(8) Sebastian, E.; Hariharan, M. Null Exciton-Coupled Chromophoric Dimer Exhibits Symmetry-Breaking Charge Separation. J Am Chem Soc **2021**, 143 (34), 13769–13781. https://doi.org/10.1021/JACS.1C05793/ASSET/IMAGES/LARGE/JA1C05793_0007.JPEG.

(9) Lu, T.; Chen, F. Multiwfn: A Multifunctional Wavefunction Analyzer. J Comput Chem **2012**, 33 (5), 580–592. https://doi.org/10.1002/JCC.22885;CTYPE:STRING:JOURNAL.

(10) Madjet, M. E.; Abdurahman, A.; Renger, T. Intermolecular Coulomb Couplings from Ab Initio Electrostatic Potentials: Application to Optical Transitions of Strongly Coupled Pigments in Photosynthetic Antennae and Reaction Centers. Journal of Physical Chemistry B **2006**, 110 (34), 17268–17281. https://doi.org/10.1021/JP0615398/SUPPL_FILE/JP0615398SI20060628_111419.PDF.

(11) Sun, Q.; Berkelbach, T. C.; Blunt, N. S.; Booth, G. H.; Guo, S.; Li, Z.; Liu, J.; McClain, J. D.; Sayfutyarova, E. R.; Sharma, S.; Wouters, S.; Chan, G. K. L. PySCF: The Python-Based Simulations of Chemistry Framework. Wiley Interdiscip Rev Comput Mol Sci **2018**, 8 (1), e1340. https://doi.org/10.1002/WCMS.1340;PAGEGROUP:STRING:PUBLICATION.

(12) Kubas, A.; Hoffmann, F.; Heck, A.; Oberhofer, H.; Elstner, M.; Blumberger, J. Electronic Couplings for Molecular Charge Transfer: Benchmarking CDFT, FODFT, and FODFTB against High-Level Ab Initio Calculations. Journal of Chemical Physics **2014**, 140 (10), 104105. https://doi.org/10.1063/1.4867077/351655.

(13) Löwdin, P. O. On the Non-Orthogonality Problem Connected with the Use of Atomic Wave Functions in the Theory of Molecules and Crystals. J Chem Phys **1950**, 18 (3), 365–375. https://doi.org/10.1063/1.1747632.

(14) Dogga, B.; Ananda Kumar, C. S.; Joseph, J. T.; A Kumar, C. S.; Dogga, B.; Joseph, J. T. Palladium-Catalyzed Reductive Carbonylation of (Hetero) Aryl Halides and Triflates Using Cobalt Carbonyl as CO Source. European J Org Chem **2021**, 2021 (2), 309–313. https://doi.org/10.1002/EJOC.202001328.

(15) Chen, F.; Gu, W.; Saeki, A.; Melle-Franco, M.; Mateo-Alonso, A. A Sterically Congested Nitrogenated Benzodipentaphene with a Double π-Expanded Helicene Structure. Org Lett **2020**, 22 (9), 3706–3711. https://doi.org/10.1021/ACS.ORGLETT.0C01202.

(16) Frederickson, C. K.; Barker, J. E.; Dressler, J. J.; Zhou, Z.; Hanks, E. R.; Bard, J. P.; Zakharov, L. N.; Petrukhina, M. A.; Haley, M. M. Synthesis and Characterization of a Fluorescent Dianthracenoindacene. Synlett **2018**, 29 (19), 2562–2566. https://doi.org/10.1055/S-0037-1610280/ID/BR000-1/BIB.

(17) Molecular Encapsulation of Conjugated Polymers for Organic Electronics. https://www.repository.cam.ac.uk/items/287712f4-605d-435f-a433-08ab5f93fb6a (accessed 2025-09-16).